A reevaluation of the constrained lever model in the primate feeding system

Jose Iriarte-Diaz[1,*], Amy Martin[1], and Myra F. Laird[2]

[1]Department of Biology, The University of the South, Sewanee, TN, USA
[2]Department of Basic and Translational Sciences, School of Dental Medicine, University of Pennsylvania, Philadelphia, Pennsylvania, USA

[*]Corresponding author (jairiart@sewanee.edu)

Keywords: bite force, TMJ, primate, triangle of support, jaw adductor muscles

ABSTRACT

The constrained lever model (CLM) predicts that the jaw adductor resultant muscle forces (RMF) must pass through a "triangle of support" (ToS) to prevent temporomandibular joint (TMJ) distraction during biting. The CLM defines distracting forces as perpendicular to the plane of the ToS, but the orientation of the ToS varies both within and between individuals based on bite point, gape, and differences in the height of the TMJ. We compare TMJ distractive forces estimated using a ToS plane versus a fixed, horizontal plane criterion across a range of gapes using muscle moments and forces for the three major jaw adductor muscles in 97 morphologically diverse primate species. At occlusion, 80% of the species experienced stabilizing compressive forces under a horizontal plane criterion, but only 44% of species had a RMF inside the ToS. This mismatch indicates that predictions of TMJ distraction and joint stability are highly dependent upon the comparison plane, which is challenging for comparisons between primates with varying TMJ heights, and consequently, ToS orientations. Joint stability increased with gape but varied little with taxonomy and across diet categories. These results provide strong evidence that the CLM is a poor predictor of the joint stability when the TMJs are elevated. These findings suggest future applications of the CLM should either focus on taxa with TMJs near the occlusal plane or calculate joint reaction forces directly to assess joint stability in mammals with elevated TMJs.

SUMMARY STATEMENT

Orientation of the triangle of support in the constrained lever model varies in primate species with elevated jaw joints, as in most mammals, which affects estimates of joint distraction.

INTRODUCTION

The capacity of an organism to generate bite force depends on the position of the bite point in the mandible, the size, position, and orientation of the jaw adductors, and on their ability to generate muscle force. From a biomechanical perspective, the mammalian feeding apparatus can be modeled as a lever system (Hylander, 1975) in which the bite force at a given tooth is the result of the force generated by the jaw adductor muscles multiplied by the mechanical advantage of the system, which is the ratio of the in-lever moment arm (i.e., the perpendicular distance of the line of action of the muscle to the TMJ axis, the axis connecting the left and right jaw joints) to the out-lever moment arm (i.e., the perpendicular distance from the bite point to the TMJ axis). If all other variables remain constant, the more posterior the bite point (i.e., the shorter the out-lever), the larger the bite force that can be generated. This is sometimes called the "unconstrained lever model" (Smith, 1978; Spencer, 1998, 1999; Santana et al., 2022). In contrast, a "constrained lever model" (CLM) has been proposed to prevent the distraction (i.e., the separation) of the mandibular condyle from the mandibular fossa of the cranium (Greaves, 1978, 2012; Spencer, 1999). In the CLM, the resultant muscle force (RMF) of the jaw adductor muscles must pass through the "triangle of support" (ToS), the triangle formed by the two TMJs and the biting point, to avoid tensile joint reaction forces (JRFs) that would distract the TMJs and compromise joint stability. If the RMF vector passes outside of the ToS, then the bite point acts as a fulcrum, rotating the mandible so that the TMJ on the working side (i.e., the biting side) will move away from the skull. The structure of the TMJ is not thought to be well equipped for resisting large tensile JRFs (Herring and Liu, 2001), and organisms are proposed to modulate their muscle activities to prevent tensile, distracting JRFs (Spencer, 1998). Thus, a key prediction of the CLM is that, as bite points become more posterior, the ToS becomes smaller, which eventually results in a reduction of the forces of the adductor muscles on the balancing side so that the RMF shifts toward the working side to stay within the ToS (**Fig. 1**).

An implicit condition of the CLM model is that, by having a RMF outside the ToS, the distractive forces acting on the joint are perpendicular to the plane of the ToS. Consequently, a JRF that is directed below the ToS would be considered distractive (JRF inside the purple area in **Fig. 2C**). This definition of distracting forces based on the ToS plane, henceforth referred as the 'ToS plane criterion', is often used in finite element analysis (FEA) to assess the stability of the jaw joint (e.g., Smith et al., 2015; Ledogar et al., 2016; Mitchell, 2019). However, as noted by others (e.g., Spencer, 1995; Ledogar et al., 2025), this definition of distracting forces varies with the orientation of the ToS plane. If we compare the mandibles of a lemur (*Lemur catta*) and gorilla (*Gorilla gorilla*), the lemur TMJ is similar in height to the occlusal row (**Fig. 2A,B**), but the gorilla TMJ is high above the occlusal row (**Fig. 2C,D**). This means that the ToS plane differs in orientation for these species, and the exact same JRF would be considered distractive for gorillas but not for lemurs (**Figs. 2A,C**). This variation in ToS plane orientation makes it challenging to compare joint stability between groups with varying TMJ heights. However, defining a constant plane, such as a 'horizontal plane criterion,' allows JRFs to be compared between groups varying in TMJ height, as illustrated by a lemur (**Fig. 2B**) and gorilla (**Fig. 2D**).

The calculation of the biomechanical parameters of the CLM is highly dependent on the accurate estimation of the muscle adductor reaction force. As pointed out by Spencer (1999), several factors can affect the location of the RMF. One factor is the differential force capability of each adductor muscle, either by having different physiological cross-sectional areas (PCSA, a proxy of the muscle's maximal tetanic force capacity) or by differential neural activation of the muscles. For example, if the temporalis has a larger PCSA or is more active than the masseter and medial pterygoid, then the position and direction of the temporalis force vector will have a larger effect on the location of the RMF. Another factor that could influence the location of the RMF is the effect that gape can have on the direction of the muscle force vectors. The CLM is usually applied assuming that the mandible is in occlusion (i.e., a 0° gape). However, it is safe to assume that most animals bite food using some degree of gape, especially when using their molars. Spencer (1999) theorized that, as gape increased, the RMF vector of the masseter would intersect the occlusal plane more posteriorly while the RMF of the temporalis would intersect more anteriorly, and that the overall RMF vector would move anteriorly with gape, making it more likely to fall outside the triangle of support.

Biting with any degree of gape introduces additional effects on the biomechanical parameters of the CLM. Increased gape affects the ability of the muscle fibers to generate force due to the skeletal muscle's length-tension relationship, as any skeletal muscle has an optimal length at which it can produce a maximal amount of active force. If the muscle fiber lengthens or shortens from that optimum, the muscle force also decreases (Huxley and Niedergerke, 1954; Gordon et al., 1966). However, the influence of this tradeoff between muscle length and force generation on the location of the RMF vector is unclear, considering that not all muscles, and not all sections of a given muscle, respond the same way to a change in gape. For example, the posterior fibers of masseter are closer to the jaw joint and experience smaller relative changes in fiber length (i.e., strain) than more anterior fibers of masseter that are farther from the joint (Iriarte-Diaz et al., 2017). These posterior fibers are therefore less affected by changes in force capability than anterior fibers. It is important to note that certain morphological and ecological traits can affect the degree of gape that an animal can achieve. For example, the height of the TMJ is negatively correlated with maximum gape and with the ability of the masseter to stretch, which provides a primary constraint on gape (Herring and Herring, 1974). This means that animals with TMJs located at the occlusal row tend to have larger gapes and associated changes in muscle architecture to facilitate large gapes, e.g., longer fiber lengths. For example, gouging callitrichid primates (*Calithrix jacchus*) have larger gapes and longer masseter muscle fibers compared to non-gouging callitrichids (*Saguinus oedipus*; Vinyard et al., 2009). Finally, both the ability to gape the jaw and the optimal length of active force production are related to diet. Maximum gape constraints diet by determining the maximal size of food accessible in birds, bats, and primates (Wheelwright, 1985; Perry and Hartstone-Rose, 2010; Santana, 2016; Fricano and Perry, 2019). Frugivorous strepsirrhines tended to consume larger blocks of food compared to folivorous strepsirrhines corresponding with longer jaw lengths, shorter TMJ heights, and longer muscle fiber lengths (Perry, 2008; Perry and Hartstone-Rose, 2010), and hard object-feeding species tend to have TMJs located high above the occlusal plan to increase the length of their muscle moment arms (Spencer, 1995; Taylor, 2002; Constantino, 2007; Terhune, 2011).

The goal of this study is to revisit the concept of ToS in the context of morphological configurations where TMJs are above the occlusal plane and evaluate the effects of gape, diet, and phylogeny on the biomechanics and stability of the TMJ. Elevated TMJs are the most common configuration in mammals, and we use primates as a model mammalian order in which to study the effects of this variation. While most primates have elevated TMJs, some strepsirrhines and *Erythrocebus patas*

monkeys have TMJs that are even with the occlusal plane (Terhune, 2011). The phylogeny of primates is well studied (Arnold et al., 2010), and the order exhibits large variation in gape (Perry and Hartstone-Rose, 2010; Hylander, 2013; Laird et al., 2023a,b, 2024). Primates also have diverse diets ranging from dedicated folivores to frugivores, omnivores, and insectivores (e.g., Perry and Hartstone-Rose, 2010). As such, we expect groups like the Pitheciids and Cebids to have high distractive forces and RMF values outside of the ToS because of their mechanically challenging diets, moderate gapes, and high TMJs (Terhune, 2011), and primates such as *Hapalemur* provide points of comparison with their lower TMJ morphological configuration but relatively large gape and mechanically challenging diet (Yamashita et al., 2009). Using a comparative dataset encompassing all major primate clades, we explore the following questions:

1. How does the position of the RMF with respect to the ToS relate to the reaction forces applied to the working-side TMJ?
2. How are the JRFs acting on the TMJs affected by gape?
3. How are the JRFs acting on the TMJs affected by muscle force estimations?
4. What are the effects of diet and phylogeny on the biomechanics and stability of the TMJ?

MATERIALS AND METHODS

Sample

We collected cranium and mandible 3D models from 167 individuals (81 females, 75 males, 11 unknown sex), spanning 97 primate species, including all primate families (except Tarsiidae; **Dataset 1**). Forty-three species were represented by just one individual, and the other 54 species were represented by multiple individuals (between two and five). Of the 54 species with multiple individuals, 45 were represented by at least one male and one female. All individuals were adults with no obvious craniodental pathological conditions, and their most posterior molar (either M2 or M3, depending on the taxon) was present and in occlusion. All individuals were obtained from public repositories such as MorphoSource or directly from scans provided by institutions such as the Field Museum (see **Dataset 1**). All original data were either CT scans or 3D models as PLY or STL files, and the CT scans were segmented using 3D Slicer (Fedorov et al., 2012) to generate STL meshes.

Model preparation

The 3D meshes of the cranium and mandible were imported into Geomagic Wrap 2017 for cleaning and to reorient them so the origin of the model is located between left and right temporomandibular joints (TMJs), that the *Y*-axis is oriented along the TMJ axis (the line connecting the two TMJs), and that the *X*-axis is parallel to the occlusal plane, defined by the occlusal surface of the molars and premolars (**Fig. 3A**). After the models were oriented, the meshes were imported into MATLAB, where the jaw adductors (i.e., superficial masseter, medial pterygoid, and temporalis) were mapped onto the models using custom MATLAB scripts (previously described in Iriarte-Diaz et al., 2017; Laird et al., 2024). Briefly, each muscle was modeled on either the left or the right side of the skull using a series of seven anterior to posterior equidistant muscle segments (**Fig. 3B**). Sensitivity analyses indicated that the number of segments modeled have little effect on the estimation of JRFs (**Fig. S2**). Each of these segments represent a muscle-tendon unit (MTU) and were created by connecting lines between the cranial and mandibular attachments that wrapped the surface of the model. These virtual muscle segments were then calculated at different gapes by virtually rotating and translating the mandible, with gapes ranging from 0 degrees (i.e., at occlusion) to 40° gape, at 5° increments. These virtual muscle segments allow us to estimate the position and direction of muscle force at different gapes for all individuals.

Determination of bite and joint reaction forces

To assess stability, we estimated the reaction forces at both the working- and balancing-side TMJ joints using a free-body analysis of masticatory force (based on Reed et al., 2016). In a static system, the moments generated by the jaw adductors on the system are balanced by moments produced by reaction forces at the bite point (i.e., bite force) and the TMJs. To derive the magnitude and direction of these reaction forces, we based our model on some basic assumptions. First, because adductor muscles were mapped only on one side, the contralateral muscle was assumed to be the mirror image around the *X*–*Z* plane. Second, muscles on the right and left sides are maximally activated and generate the same amount of force. This implies that the RMF will have no *Y* (mediolateral) component because they will cancel each other out, and that the force will be located along the midsagittal plane. Third, the direction of the bite force will be perpendicular to the TMJ axis. And fourth, for the calculation of joint reaction forces, we assumed that the

coordinate system was centered at the balancing-side TMJ. The origin could be defined anywhere, but by defining the origin at one of the TMJs, the moments acting at that point are zero, simplifying the derivation of the equations. In the equations below, vectors are bolded and scalars are in italics.

To begin, we calculated the moments generated by the masticatory muscles around the balancing-side TMJ as

$$\mathbf{M^M} = \begin{bmatrix} M_x^M \\ M_y^M \\ M_z^M \end{bmatrix} = \sum_{i=1}^{3} \sum_{j=1}^{7} \left[\left(\mathbf{r^{M_{i,j}}} - \mathbf{r^{J_{bs}}} \right) \otimes \mathbf{F^{M_{i,j}}} \right] \#(1)$$

where M_x^M, M_y^M, M_z^M are the moments about the *X*-, *Y*-, and *Z*-axis, respectively, $\mathbf{r^{M_{i,j}}}$ and $\mathbf{F^{M_{i,j}}}$ represent the position and the force vectors of the *j*-th segment of the *i*-th muscle, $\mathbf{r^{J_{bs}}}$ is the position vector of the balancing-side TMJ, and $\otimes$ represents the cross-product.

This mechanical model estimates the magnitude of the bite force as:

$$F^B = \frac{-M_y^M}{d_z^B \sin\theta \; - d_x^B \cos\theta} \#(2)$$

where d_x^B and d_z^B are the anteroposterior and superoinferior distances of the bite point to the balancing-side TMJ, and θ is the ToS plane angle, the angle between the ToS plane and the horizontal, in sagittal view (**Fig. 4A**). The ToS plane is the plane defined by the two TMJs and the bite point.

The *X* (horizontal) and *Z* (vertical) components of the working-side joint reaction forces were calculated as:

$$F_x^{Jws} = \frac{M_z^M - d_y^B F^B \sin\theta}{d_y^{Jws}} \#(3)$$

$$F_z^{Jws} = \frac{-M_x^M - d_y^B F^B \cos\theta}{d_y^{Jws}} \#(4)$$

where d_y^B and d_y^{Jws} are the lateral distances from the balancing-side TMJ of the bite point and the working-side TMJ, respectively.

Finally, the *X* and *Z* components of the balancing-side joint reaction forces are calculated as

$$F_{\mathrm{x}}^{\mathrm{Jbs}} = -F_{\mathrm{x}}^{\mathrm{Jws}} - F^{\mathrm{B}} \sin\theta - \sum_{i=1}^{3}\sum_{j=1}^{7} F_{\mathrm{x}}^{\mathrm{M_{i,j}}} \quad \#(5)$$

$$F_{\mathrm{z}}^{\mathrm{Jbs}} = -F_{\mathrm{z}}^{\mathrm{Jws}} - F^{\mathrm{B}} \cos\theta - \sum_{i=1}^{3}\sum_{i=j}^{7} F_{\mathrm{z}}^{\mathrm{M_{i,j}}} \quad \#(6)$$

where $F_{\mathrm{x}}^{\mathrm{M_{i,j}}}$ and $F_{\mathrm{z}}^{\mathrm{M_{i,j}}}$ are the horizontal and vertical components, respectively, of the muscle force of the *j*-th segment of the *i*-th muscle. For a complete derivation of these equations, see the

Supplementary Material and Methods.

Because we are comparing species of different sizes, we calculated relative joint reaction forces by dividing them by the magnitude of the RMF vector, so that all forces are unitless and can be considered as a fraction of the RMF.

In this study, in addition to using the ToS plane criterion derived from the CLM, we also defined distracting forces when the vertical component of the JRF ($F_{\mathrm{z}}^{\mathrm{Jws}}$) is positive, defined by a plane perpendicular to the occlusal plane and independent of the inclination of the ToS plane. We refer to this as the 'Horizontal plane criterion'. To compare the results from the horizontal plane criterion with the results from the ToS plane criterion, we calculated the component of the JRF perpendicular to the ToS plane ($F_{\perp\mathrm{ToS}}^{\mathrm{Jws}}$) as

$$F_{\perp\mathrm{ToS}}^{\mathrm{Jws}} = -F_{\mathrm{x}}^{\mathrm{Jws}} \sin\theta + F_{\mathrm{z}}^{\mathrm{Jws}} \cos\theta \quad \#(7)$$

where positive values indicate distracting forces according to the oblique ToS force criteria.

To validate these results, we calculated bite and joint reaction forces from finite element models of the mandibles of nine species used in this study, three from each major clade. These results demonstrate that our mathematical model accurately captures the trends in joint reaction forces with changes in gape (**Fig. S3**).

Determination of the location of the RMF

The RMF vector, $\mathbf{F}^{\mathbf{RMF}}$, was calculated as

$$\mathbf{F}^{\mathbf{RMF}} = \sum_{i=1}^{3}\sum_{j=1}^{7}\mathbf{F}^{\mathbf{M}_{i,j}} \#(8)$$

To determine the location of the RMF vector so that it accurately replicates the bite and JRFs obtained in **eqs. 2-6**, we calculated the perpendicular distance from the TMJ axis (d^{RMF}) that the $\mathbf{F}^{\mathbf{RMF}}$ must be to generate the same M_y^{M} (i.e., the bite-force producing moment) from **eq.1** as

$$d^{\mathrm{RMF}} = \frac{M_y^{\mathrm{M}}}{|\mathbf{F}^{\mathbf{RMF}}|\sin\theta\ - |\mathbf{F}^{\mathbf{RMF}}|\cos\theta} \#(9)$$

so that the position of the RMF vector on the TMJ-bite plane is $\mathbf{r}^{\mathbf{RMF}} = [d^{\mathrm{RMF}}\cos\theta\ ,0, d^{\mathrm{RMF}}\sin\theta\ ]$. The RMF angle ($\phi$) is defined as the angle between the RMF vector and the vertical, in sagittal view (**Fig. 4A**).

To compare the location of the RMF between species of different sizes, we calculated a relative RMF distance ($d_{\mathrm{rel}}^{\mathrm{RMF}}$) as

$$d_{\mathrm{rel}}^{\mathrm{RMF}} = \frac{d^{\mathrm{RMF}} - d^{\mathrm{ToS}}}{d^{\mathrm{ToS}}} = \frac{d^{\mathrm{RMF}}}{d^{\mathrm{ToS}}} - 1 \#(10)$$

where d^{ToS} is the perpendicular distance of the anterior edge of the ToS from the TMJ axis (**Fig. 4B**). In this relative distance, negative values indicate that the RMF is located inside the ToS, while positive values indicate that the RMF is located outside the ToS.

Factors affecting joint reaction forces

Relative muscle force effect:

The joint reaction forces calculated in **eqs. 3-6** depend on the magnitude of the muscle forces acting on the system. In our model, we assume that the jaw adductor muscles are maximally activated, generating maximal tetanic force. Maximum tetanic muscle forces are often calculated by estimating the muscle's physiological cross-sectional area (PCSA) and multiplying it by the specific tension of skeletal muscle (Powell et al., 1984). Estimating the PCSA of the jaw adductors is an elaborate process that either involves careful dissections (e.g., Taylor and Vinyard, 2013) or imaging using special staining techniques (e.g., Dickinson et al., 2019). Although the number of primate species for which PCSA information is available has steadily increased, there is still a lack

of these data for many species, especially for the medial pterygoid (see Taylor et al., 2025 for a review). Additionally, recent analyses of muscle physiology in primates show that there is substantial intra- and intermuscular heterogeneity in fiber type, and consequently, in specific muscle tension (Holmes and Taylor, 2021; Taylor et al., 2025). In this study, we focus on the relative joint reaction forces with respect to the total RMF, rather than estimating the absolute bite and reaction forces. This means that the most important factor for these analyses is not the absolute muscle forces generated, but the relative amount of force between muscles. As a consequence, the magnitude of the force generated by an individual muscle segment ($F^{\mathrm{M_{i,j}}}$) in eq. 1 was defined as

$$F_{\max}^{\mathrm{M_{i,j}}} = \frac{F_{\max}^{\mathrm{M_i}}}{7} \#(11)$$

where $F_{\max}^{\mathrm{M_i}}$ is the fraction of the total maximal tetanic force produced by the i-*th* muscle, divided by the number of modeled segments, which in our case is 7. So, if the $F_{\max}^{\mathrm{M_i}}$ is 0.3 for the masseter, 0.25 for the medial pterygoid, and 0.45 for the temporalis, this means that the masseter generates 30% of the total muscle force, the medial pterygoid generates 25%, and the temporalis 45%. To assess the effect of variation in the relative muscle force, we calculated the reaction forces for 182 different sets of $F_{\max}^{\mathrm{M_i}}$, ranging from 0.2 to 0.6 for each muscle, so that the sum of the three $F_{\max}^{\mathrm{M_i}}$ is 1. The sets of relative muscle forces likely represent a larger range of forces than observed in nature. Finally, to evaluate the effect of using different relative muscle forces on the estimation of joint reaction forces, we calculated the difference in reaction forces for each muscle condition to a reference condition ($F_{\max}^{\mathrm{ref}}$) where the muscles produce the same relative force (i.e., $F_{\max}^{\mathrm{Masseter}} = F_{\max}^{\mathrm{Med.\ Pterygoid}} = F_{\max}^{\mathrm{Temporalis}}$ = 1/3).

Length-Tension (L–T) effect:

The force-generating capacity of any muscle depends on its contractile properties and varies with operating length. The relationship between the muscle length and its capacity to generate maximum tetanic force is known as the length-force (or length-tension) curve. In this relationship, there is an optimal length at which the muscle can produce maximal force. If the muscle either shortens or lengthens from this optimal length, the muscle force decreases. In the case of the jaw adductor muscles, their length-force curve depends on gape. As the mandible opens and gape increases, the jaw adductor muscle fibers stretch, changing where on the length-force curve

muscles operate. We used a simple musculoskeletal model to estimate how much changes in gape would affect muscle force generation. This model is explained in detail in Laird et al. (2024). Briefly, the model assumes a pennated muscle where the pennation angle increases with muscle shortening while maintaining a constant muscle thickness. In this model, the maximum force that an individual muscle segment can generate for a given gape angle ($F_{(\mathrm{gape})}^{\mathrm{M_{i,j}}}$) is defined as:

$$F_{(\mathrm{gape})}^{\mathrm{M_{i,j}}} = F_{\max}^{\mathrm{M_{i,j}}}\, \hat{f}_{(\mathrm{gape})}^{\mathrm{M_{i,j}}} \cos\alpha_{(\mathrm{gape})} = \frac{F_{\max}^{\mathrm{M_i}}}{7}\, \hat{f}_{(\mathrm{gape})}^{\mathrm{M_{i,j}}} \cos\alpha_{(\mathrm{gape})} \quad \#(12)$$

where $\alpha_{(\mathrm{gape})}$ is the pennation angle for a given gape, and $\hat{f}_{(\mathrm{gape})}^{\mathrm{M_{i,j}}}$ is the normalized active force that the muscle can generate from the length-force curve at a given gape (**Fig. S4**). The term (gape) indicates the variable changes with the gape angle. For this analysis, we assume that $F_{\max}^{\mathrm{M_i}}$ is the same for all muscles as is set to $F_{\max}^{\mathrm{ref}}$, which does not change with gape. How much both the pennation angle α and $\hat{f}^{\mathrm{M_{i,j}}}$ change depend on how much individual muscle segments change with gape. From the virtual 3D muscle models, we can easily calculate the change in MTU length with gape. However, in pennated muscles, how much the muscle fiber length changes for a given MTU length change depends on the architectural configuration of the muscle. Here, we calculated the muscle fiber strain, ε_f (i.e., normalized change in muscle fiber length) as

$$\varepsilon_{\mathrm{f}} = 1 - \sqrt{\frac{(L_{\mathrm{f}} \sin\alpha)^2 + \left(L_{\mathrm{f}} \cos\alpha + \Delta m_{(\mathrm{gape})}\right)^2}{{L_{\mathrm{f}}}^2}} \#(13)$$

where L_f and α are the fiber length and the pennation angle at occlusion (i.e., 0° gape), and $\Delta m_{(\mathrm{gape})}$ is the change in MTU length from occlusion for a given gape angle. The pennation angle for a given gape ($\alpha_{(\mathrm{gape})}$) was calculated as

$$\alpha_{(\mathrm{gape})} = \left(\frac{L_{\mathrm{f}} \cos\alpha + \Delta m_{(\mathrm{gape})}}{\varepsilon_{\mathrm{f}} L_{\mathrm{f}}}\right) \#(14)$$

Once we know how much a muscle fiber was stretched for a given gape, we can estimate the relative active force component $\hat{f}_{(\mathrm{gape})}^{\mathrm{M_{i,j}}}$ of the length-tension curve, which also depends on the occlusal offset length (ΔL_{occ}), the difference in normalized fiber length between the muscle fiber at occlusion and when maximum force is generated (**Fig. S4**).

Tendons and aponeuroses compliance was assumed to have a negligible effect on the changes in MTU length, considering that the estimated ratio of tendon to fiber length of the jaw adductor muscles falls below three in some primates (Laird et al., 2024), a critical value under which tendons can be considered stiff and non-compliant (Zajac, 1989).

Unfortunately, we do not have jaw adductor muscle architecture data, nor do we know what the ΔL_{occ} is for many of the primate species included in this study. So, to evaluate the effect that gape-related changes in muscle force capabilities have on the joint reaction forces, we tested multiple combinations of L_f changing from 50% of the MTU length to 80% of the MTU length (in 3% increments) and ΔL_{occ} ranging from 0.1 to 0.5 (in 0.03 increments), resulting in 144 different conditions. We also modeled the effect of variation of pennation angles, but this had a minimal effect on muscle force generation, so we used the same pennation angle at occlusion (15 degrees) for all conditions.

Effect of individual muscles

To evaluate the effect that each of the three individual jaw adductors have on the stability of the TMJ, we defined the effect for a given muscle as the difference between the F_z^{Jws} calculated the selected muscle produces the largest force relative to the other two jaw adductor muscles, and the F_z^{Jws} calculated when all of the jaw adductor muscles generate the same relative force. For example, to calculate the effect of the temporalis, we calculate the JRF using $F_{max}^{M_i}$ = 0.6 for the temporalis and $F_{max}^{M_i}$ = 0.2 for both the masseter and medial pterygoid, and then subtract the JRF calculated when using $F_{max}^{M_i} = F_{max}^{ref}$ = 0.3 for all muscles. If the effect for a muscle is positive, increased force from this muscle will result in the working-side TMJ having more positive vertical JRFs, making the joint more unstable.

Statistical analyses

All statistical analyses were carried out in RStudio with R 4.4.2 (R Core Team, 2024).

A consensus phylogenetic tree was downloaded from 10k Trees version 3 (Arnold et al., 2010). We assigned dietary preferences based on previous classifications in published literature into four

categories: folivore, folivore/frugivore, frugivore, and omnivore. The classification of diets and their source references are provided in **Dataset 1**.

To evaluate the effect of gape, clade, and diet on joint mechanical parameters, we fit a series of generalized mixed-effect linear models using the Bayesian *'brm'* function of the *brms* package (Bürkner, 2018). For these regressions, all variables were standardized. Gape angle and (gape angle)^2 were used as covariates to evaluate linear and quadratic effects, respectively. Phylogenetic effects were included as a random covariance matrix and included 'species' as a random group effect to control for repeated measures of gape angles for each species. For each response variable, we ran three different regressions: 1) a regression with only the covariates, to assess the general effect of gape on the variable; 2) a regression with both covariates, clade as a fixed effect, and the interaction of gape angle and clade; and finally, 3) a regression with both covariates, diet as a fixed effect, and the interaction effect of gape angle and diet. We did not evaluate the interaction effect between clade and diet because not all diets were observed in each clade group. We used the default priors of the brms package, assumed a Gaussian response distribution, and ran two chains, each with 10,000 iterations, 5,000 of which were warmup iterations. Model convergence was verified by ensuring that the R-hat statistic for all parameters was below 1.01 (Bürkner, 2018). Model fit was assessed using posterior predictive check plots.

To estimate the importance of fixed effects (i.e., clade or diet) on joint mechanical parameters, pairwise comparisons of levels of each fixed effect we calculated using the 'emmeans' function of the *emmeans* package (Lenth, 2025). Because regressions that included fixed effects also had an interaction effect with gape angle, we calculated the pairwise differences at three gapes (0°, 20°, and 40° gape) independently. To assess the significance of a coefficient we used the 95% highest density interval (95% HDI) to evaluate the uncertainty of the estimate (Kruschke and Liddell, 2018), the probability of direction (pd) to evaluate the existence of the effect, and the percentage in ROPE (region of practical equivalence) to evaluate the significance of the effect using the 'describe_posterior' function of the *bayestestR* package (Makowski et al., 2019a). The HDI is the interval on the posterior distribution of each coefficient estimate that contains a higher probability density than points outside the interval. The pd represents the proportion of the posterior distribution that goes in a particular direction, either positive or negative. For example, a pd of 95% indicates that 95% of sampled estimates of the coefficient are to one side of zero. An advantage of pd is that it is strongly correlated with the frequentist *p*-value, where two-sided *p*-values of 0.05

and 0.01 correspond approximately to pd values of 97.5% and 99.5% respectively (Makowski et al., 2019b). The percentage in ROPE (region of practical equivalence) is an index of significance, indicating whether the effect is large enough to be considered significant. The ROPE was set as [–0.1, 0.1] following Kruschke and Lidell's recommendation when dealing with standardized parameters (Kruschke and Liddell, 2018). As suggested by Makowski et al. (2019b), we consider this index as continuous index of significance, with the following reference values: >97.5% in ROPE as probably negligible effect (we can accept the null hypothesis); between 97.5% and 2.5% in ROPE as of undecided significance; <2.5% in ROPE as probably significant; and <1% in ROPE as significant (we can reject the null hypothesis).

The phylogenetic signal lambda (λ) was estimated for all models as the proportion of the total variance attributable to phylogenetic variance, using the 'hypothesis' method following the recommendations in the vignettes of the *brms* package. A value close to 0 indicates trait evolution independent of phylogeny (i.e., no phylogenetic signal), while values close to 1 indicate strong phylogenetic signal.

To assess the performance of the models, we calculated the marginal R^2, which measures the proportion of variance explained by fixed factors (i.e., gape angle, clade, and diet), and conditional R^2, which measures the proportion of variance explained by fixed and random effects (i.e., phylogeny and species effects), using the 'r2_bayes' function of the *performance* package (Lüdecke et al., 2021).

To evaluate factors that might affect whether or not the working-side joint reaction forces are compressive or tensile when biting on the posterior molars, we calculated phylogenetic regressions between the ToS plane angle, the RMF angle at occlusion (i.e., at 0° gape), and the vertical JRF on the working-side TMJ (F_z^{Jws}). Both regressions were calculated using the 'brm' function with the working-side JRF as the dependent variable and either the ToS plane angle or the RMF angle as the independent variable, using the same priors and iterations parameters as indicated above.

Finally, descriptive statistics of angular data were calculated using the *circular* package (Agostinelli and Lund, 2024).

RESULTS

We first present the results for a single species, *Pan paniscus*, as an example, and then we present the results for all species in a phylogenetic framework.

JRFs and RMF position in *Pan paniscus*

When considering only the reference muscle configuration (i.e., when all adductor muscles generate the same relative muscle force), the direction of the JRF varies with gape, moving from a posteriorly and superiorly directed force at occlusion (i.e., 0° gape) to a mostly vertically directed force at 40° gape (**Fig. 5A**). Because there is a vertically directed force component at all gapes, according to the horizontal plane criterion, the working-side TMJ experiences only compressive, stabilizing forces that keep the mandibular condyle pushed against the mandibular fossa of the cranium. Interestingly, the RMF position also changes with gape, moving posteriorly as gape increases, from 0.16 (i.e., outside the ToS) at occlusion to 0 (i.e., at the edge of the ToS) at 40° gape (**Fig. 5A**), which would suggest mostly tensile, distracting forces at the working-side TMJ as predicted by the CLM.

To evaluate the importance of the relative muscle force effect, we plotted histograms of the distribution of the JRFs and RMF positions for all sets of muscle force configurations. The distributions show that the muscle force configuration does affect both the working-side vertical JRF and the RMF position, and that both variables become more negative with gape (**Fig. 5B,C**). However, the magnitude and direction of the effect of muscle force configuration are different for the JRF and the location of the RMF. For the JRF, the distribution is narrower and slightly positively skewed at small gapes and slightly negatively skewed at large gapes (**Fig. 5B**). In contrast, the distribution of the RMF position on the ToS plane is wider, positively skewed, and includes vectors located both inside and outside of the ToS at all gapes (**Fig. 5C**).

The relative muscle force effect shows substantial variation around the reference muscle configuration for *Pan paniscus* (**Fig. S5A**). The range of the effect remains relatively constant between 0 and 15° gape and then increases slowly with gape. In contrast, the effect of changes in muscle force generation due to changes in gape (i.e., L–T effect) shows smaller ranges that increase with gape (**Fig. S5B**).

JRF and RMF position at occlusion across primates

Of the 97 species sampled in this study (**Fig. 6A**), 78 species (80%) exhibit compressive, stabilizing vertical forces, according to the horizontal plane criterion, at their working-side TMJ at occlusion (i.e., 0° gape) (**Fig. 6B**). Of the 19 species that show distracting forces, one is a catarrhine (*Trachypithecus phayrei*), six are platyrrhines (*Callimico goeldii*, *Cebus albifrons*, *C. apella*, *C. capucinus*, *C. olivaceous*, and *Saguinus fuscicollis*), and 12 are strepsirrhines (*Daubentonia madagascariensis*, *Eulemur flavifrons*, *Galago alleni*, *Hapalemur griseus*, *Indri Indri*, *Loris tardigradus*, *Microcebus murinus*, *Nycticebus coucang*, *N. pygmaeus*, *Otolemur crassicaudatus*, *Perodicticus potto*, and *Varecia variegata*). These species represent 2% of catarrhines, 24% of platyrrhines, and 57% of strepsirrhines. Thus, we would expect a similar proportion (80%) of species where the RMF is located inside the ToS. However, we see that only 44% of all species have the RMF inside the ToS (**Fig. 6C**). The difference between the JRF and the expected location of the RMF is not equally spread among clades. In 37% of catarrhines, 56% of platyrrhines, and 14% of strepsirrhines, the RMF position with respect to the ToS is different from what would be expected from their JRF.

In contrast, when comparing the results using the ToS plane criterion with the predictions from the RMF position, we observe a much better match, with 97% of the species exhibiting JRFs that match the expectations from the location of the RMF. Four species exhibit JRFs contrary to the expectations from the RMF position (*Callithrix jacchus*, *Gorilla beringei*, *Macaca arctoides*, and *Saimiri sciureus*). In all these cases, the RMF was outside the ToS but close to the edge ($d_{\mathrm{rel}}^{\mathrm{RMF}} <$ 0.01), and the reaction forces were compressive but small ($F_{\perp \mathrm{ToS}}^{\mathrm{J_{ws}}} >$ –0.006).

Effect of gape on the joint reaction forces

The summary statistics of the Bayesian regressions of the JRFs are in **Tables S1** and **S2**. The horizontal component of the JRF on the balancing side shows mostly negative forces, with the magnitude of the force increasing with gape from –0.03 at 0° gape to –0.18 at 40° gape (**Fig. 7A**, top left panel). The vertical component of the balancing-side JRFs, however, is strongly negative, with a slight increase in magnitude with gape, from –0.35 at 0° gape to –0.37 at 40° gape (**Fig. 7A**, top right panel). All this results in a JRF vector that is, on average, almost vertical at occlusion (JRF angle at

0° gape = –94.5 ± 6.4° [circular mean ± circular SD]; **Fig. S6B**) and becomes more posteriorly directed at larger gapes (JRF angle at 40° gape = –115.3 ± 4.7°; **Fig. S6C**).

In contrast, the JRFs show a different pattern on the working side. The horizontal force component of the JRF is mostly positive, remaining relatively constant at around 0.10 up to 20° gape, and decreasing to 0.01 at 40° gape (**Fig. 7A**, bottom left panel). The vertical component of the working-side JRF is mostly negative and increases linearly in magnitude with gape, from –0.05 at 0° gape to –0.25 at 40° gape (**Fig. 7A**, bottom right panel). At 0° gape, 19 species (20% of the total species) exhibited positive/distractive forces as mentioned in the previous section. At 10° gape, only 3 strepsirrhine species (*H. griseus*, *O. crassicaudatus*, and *P. potto*) showed positive vertical forces, and by 15° gape, no species exhibited distracting vertical forces. This results in a JRF vector that is, on average, directed forward and downward at occlusion (mean JRF angle at 0° gape = –26.8 ± 36.6°; **Fig. S6D**) and moving backwards to an almost vertically directed vector at large gapes (mean JRF angle at 40° gape = –87.4 ± 5.3°; **Fig. S6E**).

Effect of gape on the RMF position

The summary statistics of the Bayesian regressions of the position of the RMF are in **Table S3**. The position of the RMF with respect to the ToS shows a similar pattern with gape, with the RMF moving posteriorly, closer to the TMJ axis, as gape increases (**Fig. 7B**). On average, the RMF is located just outside of ToS ($d_{\mathrm{rel}}^{\mathrm{RMF}}$ = 0.03) at 0° gape and moves well into the ToS ($d_{\mathrm{rel}}^{\mathrm{RMF}}$ = –0.22) at 40° gape. At 0° gape, 55 species (57% of the total species) exhibit RMF vectors located outside the ToS. Except for *Callicebus torquatus*, whose RMF was consistently outside of the ToS at all gapes, all other species have their RMF located within the ToS by 35° gape.

Effect of gape on factors that affect the working-side vertical joint reaction force

The summary statistics of the Bayesian regressions of the factors that affect the working-side vertical JRF are shown in **Tables S4** and **S5**. The range of the relative muscle force effect shows a curvilinear relationship with gape, remaining relatively constant around 0.11 from 0° to 15° gape and then increasing to 0.14 at 40° gape (**Fig. 8A**, left panel). In contrast, the range of the L–T effect increased linearly with gape, from 0.03 at 5° gape to 0.06 at 40° gape (**Fig. 8A**, right panel).

In terms of individual muscle effects, we see that each muscle affects the joint stability in different ways. The masseter makes the working-side vertical JRF more positive at all gapes and increases with gape, decreasing the stability of that joint (**Fig. 8B**, left panel). In contrast, the medial pterygoid makes the working-side vertical JRF more negative at small gapes and has little effect at large gapes (**Fig. 8B**, middle panel). Finally, the temporalis makes the working-side vertical JRF more positive at small gapes and more negative at large gapes (**Fig. 8B**, right panel).

Effect of clade and diet on the mechanics of the jaw

Plots of regression models including the effect of either clade or diet are in **Figs. S7**, **S10**, **S12**, and **S14**, and the plots of the posterior distributions of the pairwise comparisons for each factor are shown in **Figs. S8-S9, S11, S13,** and **S15**. Because the slope of the levels of each factor with gape was allowed to vary, we estimated the differences between clade and dietary categories at 0°, 20°, and 40° gapes. The only consistent differences between clades across gapes were in the vertical component of the working-side JRF, where there is strong evidence that strepsirrhines have more positive working-side vertical JRFs than catarrhines (**Figs. 6B**, **S7D**, and **S9B**). For the effect of diet, the only consistent differences were in the relative muscle force and L–T effect ranges, with folivores having greater effects than frugivores/folivores species (**Figs. S12** and **S13**).

In terms of the effect that individual muscles have on the vertical force component of the working-side JRF, we observed that the masseter has a significantly smaller effect in frugivores/folivores than in both frugivores and folivores, and maybe omnivores, but this comparison is not significant (**Figs. S14A** and **S15A**). For the medial pterygoid, the effect of this muscle on the vertical working-side JRF was larger in frugivores/folivores than in omnivores (**Figs. S14B** and **S15B**). No significant differences were observed for the temporalis.

Relationship between RMF angle, ToS plane angle, and joint reaction forces

The ToS plane angle is significantly steeper in catarrhines than in strepsirrhines and is also significantly steeper in folivores than both omnivores and frugivores/folivores (**Figs. S16A** and **S17A**).

The RMF angle tends to be more anteriorly oriented in both platyrrhines and strepsirrhines than catarrhines, but the differences are not significant (**Fig. S16B** and **S17B**). There is no difference in RMF angles between dietary groups (**Fig. 16B** and **S17B**).

The relationship between RMF angle and the working-side vertical JRF was not significant (**Fig. S18A**; slope median = 0.08, 95% HDI = [–0.11, 0.27], pd = 80%, 80% in ROPE, marginal R^2 = 0.01). In contrast, the relationship between the ToS plane angle and the working-side vertical JRF shows a weak/moderate but significant positive relationship (**Fig. S18B**; slope median = 0.32, 95% HDI = [0.19, 0.46], pd = 100%, 0% in ROPE, marginal R^2 = 0.27).

A weak negative relationship exists between RMF angle and ToS plane angle (slope median = –0.47, HDI = [–0.71, –0.23], pd = 100%, 0% in ROPE, marginal R^2 = 0.16).

DISCUSSION

The CLM was proposed to explain how the jaw adductor muscle forces are arranged to avoid tensile (distractive) forces at the TMJ and to predict force reductions in these muscles depending on bite point location within the ToS (Greaves, 1978, 2012; Spencer, 1999). Among primates, force predictions resulting from the ToS have been related to dietary adaptations (e.g., Wright, 2005), dental eruption and life history (e.g., Singleton, 2015; Glowacka and Schwartz, 2021), and used in finite element models of the feeding system (e.g., Smith et al., 2015; Ledogar et al., 2016a). We present the first comparative data testing differences in the joint reaction forces at the TMJ with the RMF and ToS and the effects of gape and muscle force estimations across a large sample of taxonomically and dietarily variant primates. Here, we discuss the implications of our results on joint stability, taxonomic and dietary variation, and propose a revised approach to the ToS for future research.

Determination of TMJ stability is criterion-dependent

Our results show that assessing whether the working-side TMJ will experience compressive (stabilizing) or tensile (distracting) vertical forces in primates depends on the criterion used for defining distracting forces. In our sample, 56% of species have a the RMF at occlusion that falls outside the ToS, suggesting the TMJ is under distraction according the ToS plane criterion from the CLM. In contrast, only 20% of the species would exhibit distracting forces according to the horizontal plane criterion. This mismatch is due to differences in how distracting forces are defined. Based on the horizontal plane criterion, we define JRFs as distracting when they have a downward vertical force component, which is the same for all species. In contrast, the ToS plane criterion defines distracting forces as being perpendicular to the plane of the ToS, so that the orientation of the distracting forces can vary among species due to differences in the inclination of the ToS plane. With that in mind, the location of the RMF with respect to the ToS is excellent at predicting the stability of the joint, if we assume that the ToS plane criterion of the CLM is the best way of defining the stability of the joint. At occlusion, the location of the RMF accurately predicts the presence or absence of distracting joint forces perpendicular to the ToS in 97% of species. The few species where the location of the RMF did not predict the stability of the joint, the RMF was very close to the edge of the ToS, so it is possible that the differences reflect a margin of error and that the reaction forces acting on the joints of those species are negligible.

However, we argue that the ToS plane criterion derived from the CLM is not the best way of assessing the stability of the jaw joint, and the horizontal plane criterion should be used instead. First, the definition of distracting forces is not consistent between species due to differences in the orientation of the plane of the ToS. In primates, the ToS can vary substantially from approximately horizontal in strepsirrhines to highly tilted in apes (**Fig. 2**). Furthermore, the criterion for distracting forces can vary for the same individual at different bite points, as pointed out in the FEA literature (e.g., Ledogar et al., 2025). Second, the mismatch percentages in our results suggest there are cases where the ToS plane criterion incorrectly classifies JRFs as distractive or non-distractive (**Fig. 9**). In cases where the direction of the JRF vector lies above the ToS plane but below the horizontal plane, the ToS plane criterion would determine that the joint is stable and under compression because the JRF component perpendicular to the ToS plane is directed towards the cranium (purple arrow in **Fig. 9A**). Nonetheless, because the JRF vector is below the horizontal plane, there is still a vertical force component that pulls the mandibular condyle away from the cranium (green

arrow in **Fig. 9A**), creating a distracting condition. In contrast, in cases where the direction of the JRF vector lies below the ToS plane but above the horizontal plane, the ToS plane criterion will determine that the joint experiences a distracting force (purple arrow in **Fig. 9B**). In these cases, there will be a vertical force component pushing the mandibular condyle towards the cranium that will prevent distraction of the joint (green arrow in **Fig. 9B**). The region of mismatch between the vertical force and the oblique ToS force criteria for joint stability (purple areas in **Fig. 9**) increases with steeper ToS planes. This could explain why FEA studies have shown that modern humans and some chimpanzees experience distracting forces in the working-side TMJ during molar biting (Ledogar et al., 2016b, 2025; Cook et al., 2021), contrary to our results (**Fig. 6B**).

The horizontal plane criterion that we propose works well in primates despite TMJ shape variability across the species as the cranial portion of the joint is always open inferiorly (Terhune et al., 2022). However, this criterion might not work on other mammals such as carnivores with hinge-like TMJs (Crompton et al., 2006), where the mandibular fossa might enclose the mandibular condyle inferiorly, changing the axis of joint instability (Clausen et al., 2008).

Clade-level differences

The largest clade-level difference was that strepsirrhines experience more positive working-side vertical JRFs (F_z^{Jws}) relative to catarrhines, which indicates that strepsirrhines are more prone to distracting forces at their TMJs. More than half of the strepsirrhines exhibit distracting forces at occlusion compared to only 2% of catarrhines. The prevalence of distractive joint forces in strepsirrhines may reflect aspects of their mandibular morphology. First, the majority of strepsirrhines have an unfused fibrocartilaginous mandibular symphysis that allows for limited independent movement for the right and left hemimandibles (Ravosa and Vinyard, 2020), but we note that symphyseal fusion patterns in strepsirrhine primates do not perfectly map onto species with positive vertical JRFs (Scott et al., 2012). Another explanation as to why strepsirrhines exhibit more unstable TMJs compared to catarrhines might be that the temporalis has a large effect on strepsirrhines. Strepsirrhines have relatively larger temporalis PCSAs compared to catarrhines (Taylor et al., 2025), and this temporalis attaches to a pronounced coronoid process to facilitate relatively large gapes and increased leverage (Perry, 2008). Although we did not find significant differences in the effect of the temporalis on the F_z^{Jws} between clades, the temporalis has a

destabilizing effect by making the F_z^{Jws} more positive for most strepsirrhines (**Fig. S15C**). Although not significant, strepsirrhines tend to have more anteriorly directed RMF (**Fig. S16B**), which would move the location of the RMF forward, making the system less stable. Finally, previous studies have shown that the TMJ in strepsirrhines is closer to the occlusal plane than in anthropoids (Ravosa et al., 2000; Armfield and Vinyard, 2010). In this study, strepsirrhines had shallower ToS plane angles than catarrhines (**Fig. S16A**), and we see that the ToS plane angle is correlated with the vertical stability of the working-side TMJ (**Fig. S18**).

Outside of strepsirrhines, platyrrhines had the highest percentage of taxa with tensile distractive forces (24%) and the largest percentage of taxa with the location of the RMF with respect to the ToS differing from their JRF expectation (56%). Both strepsirrhines and platyrrhines have negative allometry in adductor fiber lengths, meaning that larger animals have shorter muscle fiber lengths, limiting stretch (Taylor et al., 2025). Platyrrhines also have negative allometry for masseter and temporalis PCSA, meaning that smaller animals are at a relative advantage for muscle stretch and gape compared to larger animals (Taylor et al., 2025). This is mostly consistent with our clade-level results in that the location of the RMF was within the ToS in most Callitrichids, the smallest platyrrhines, and for the smallest bodied platyrhines within some groups, *Saimiri* within the Cebids, for example. As expected, groups such as the Cebids and Pitheciids that have mechanically challenging diets, moderate gapes, and high TMJs (Terhune, 2011), tended to have RMFs outside of the ToS. In particular, all of the modeled Pitheciids had RMFs located outside of their ToS, which may reflect their laterally flaring zygomatics and anteriorly attaching superficial masseter muscles (Terhune et al., 2015).

Joint stability increases with gape, but diet has little effect on TMJ stability

We found that joint stability increased with gape. At occlusion, 19 species had distractive JRFs, according to the horizontal plane criterion, but no species had distractive forces above 15° gape. This increase in TMJ stability with larger gapes may reflect selection for joint stability at gapes at or above optimal force, as opposed to when the jaw is at occlusion. This selective pressure is especially relevant for large, mechanically challenging food items, which are more likely to require molar bites and wider gapes than similarly sized items processed with the anterior teeth. As such, we might have expected to find differences in TMJ stability with diet, but there were no consistent

differences in the reaction forces acting on the TMJ between diet categories across primates. While we used diet categories to test differences in TMJ stability, we acknowledge that they do not capture the substantial geographic and seasonal variation of primate diets, and that these categories do not reflect differences in food material properties (Coiner-Collier et al., 2016) or differences in feeding behaviors (Ross et al., 2012; Ross and Iriarte-Diaz, 2014). Future tests with more specific food material properties and food size data may yield a better understanding of the role of selection for joint stability at larger gapes in primates.

We did find dietary differences in the variables that affect the vertical stability of the working-side TMJ. Folivores have larger relative muscle force effect ranges than species in the frugivore/folivores group (**Fig. S13A**), which means that changes in the relative force that adductor muscles generate will have a larger effect on the F_z^{Jws} in folivores compared to frugivores/folivores. Folivores also exhibit larger L–T effect ranges than frugivores/folivores (**Fig. S13B**), which means that changes in muscle force due to variation in gape will have a larger effect on the F_z^{Jws} of folivores than in frugivores/folivores. This could be a consequence of the larger effect the masseter muscle has on F_z^{Jws} in folivores compared to that of frugivores/folivores (**Fig. S15A**), as the masseter tends to stretch more with gape than both medial pterygoid and temporalis. These results are consistent with suggestions that the jaw adductors in folivores have adaptations for undergoing repetitive loading at smaller gapes (Strait, 1997; Hogue, 2004; Lucas, 2004; Scott et al., 2012).

Limitations of the study

As with any modeling approach, there are simplifications and assumptions that may have affected our results. First, we only modeled the three major jaw adductor muscles. It is possible that the smaller muscles that were not considered may influence the stability of the joint. For example, the deep masseter, which fibers are more vertically oriented (Taylor et al., 2025), could make the RMF more posterior and increase the stability of the jaw joint. In the same vein, the superior head of the lateral pterygoid may be active during jaw closing in some primates and to stabilize the TMJ (Grant, 1973; McNamara, 1973; Hiraba et al., 2000; but see Murray et al., 2007; Murray, 2012). However, finite element analyses suggest that our model accurately captures changes in joint reaction forces (**Fig. S3**).

Second, when modeling the L–T effect, we assumed that all jaw adductor muscles reach maximal force at the same level of strain from occlusion (i.e., have the same ΔL_{occ}). Even though variation in jaw adductor ΔL_{occ} across primates is unknown, considering that the masseter tends to stretch more with gape than both the temporalis and the medial pterygoid, it is possible that there are muscle-specific differences in ΔL_{occ}.

Third, our model assumes the mandible is a solid, rigid body without considering the internal structure of the bone. Tests of load paths in Virginia opossums suggest mandibular models including internal cortical and trabecular differences best replicate bite force and strain data, but the majority of the load travels in the cortical bone (Wilken et al., 2024). We also do not consider mandibular structural differences across primates, including the presence of unfused symphyses in some strepsirrhines, even though there is good evidence to suggest that symphyseal fusion affects mandibular loading (Hylander et al., 2000; Scott et al., 2012). The addition of such features in our models complicates the mechanical environment for comparative analyses, and we suggest that finite element analyses may be better suited for testing the effects of such features.

Finally, while our analyses include 167 specimens from 97 taxa, the number of individuals representing each species is small, and it is unclear how intraspecific variation may affect the results, especially in species with strong sexual dimorphism.

Conclusions

The CLM is a widely used model for understanding the biomechanics of the mammalian feeding system (Greaves, 1978, 2012; Spencer, 1999). According to the CLM, the distracting forces acting on the joint are defined as perpendicular to the ToS plane. However, we argue that the use of the position of the RMF relative to the ToS—the central concept of the CLM—influences predictions of jaw joint stability in primates. Using the ToS to determine distraction results in inconsistent comparisons between species with differing jaw joint heights, as well as between bite locations.

To address this issue, we propose using a horizontal plane criterion to define joint stability. This criterion is consistent across different species and bite points. Our data shows that, using this horizontal plane criterion, there is significant variation in joint stability with changes in gape; however, there are only minor differences in joint stability when considering taxonomy and diet. These results suggest that future studies employing the ToS model should be limited to taxa jaw

joints situated close to the occlusal plane or should directly calculate the joint reaction forces of the system.

List of symbols and abbreviations

CLM Constrained lever model

$(d_{\mathrm{x}}^{\mathrm{B}}, d_{\mathrm{y}}^{\mathrm{B}}, d_{\mathrm{z}}^{\mathrm{B}})$ distance of the bite point from the balancing-side TMJ in the X, Y, and Z direction

$d_{\mathrm{y}}^{\mathrm{Jws}}$ distance of the working-side TMJ from the balancing-side TMJ in the Y direction

d^{RMF} perpendicular distance of the resultant muscle force from the TMJ axis

$d_{\mathrm{rel}}^{\mathrm{RMF}}$ relative position of the resultant muscle force with respect to the anterior edge of the triangle of support

d^{ToS} perpendicular distance of anterior edge of the triangle of support in the midsagittal plane

F^{B} Bite force magnitude

$F_{\mathrm{x}}^{\mathrm{Jws}}, F_{\mathrm{z}}^{\mathrm{Jws}}$ magnitudes of the horizontal and vertical working-side joint reaction forces

$F_{\mathrm{x}}^{\mathrm{Jbs}}, F_{\mathrm{z}}^{\mathrm{Jbs}}$ magnitudes of the horizontal and vertical balancing-side joint reaction forces

$F_{\perp \mathrm{ToS}}^{\mathrm{Jws}}$ magnitude of the working-side joint reaction force perpendicular to the plane of the triangle of support

$\mathbf{F}^{\mathbf{M_{i,j}}}$ 3D force vector of the *j*-th segment of the *i*-th muscle

$F_{(\mathrm{gape})}^{\mathrm{M_{i,j}}}$ maximum force that *j*-th segment of the *i*-th muscle can generate at a given gape angle

$\hat{f}_{(\mathrm{gape})}^{\mathrm{M_{i,j}}}$ normalized active force that the *j*-th segment of the *i*-th muscle can generate from the length-force relationship at a given gape angle

$F_{\mathrm{x}}^{\mathrm{M}}, F_{\mathrm{z}}^{\mathrm{M}}$ magnitude of the horizontal and vertical component of the muscle force

$F_{\mathrm{max}}^{\mathrm{M_i}}$ fraction of the maximal tetanic force generated by the *i-th* muscle

$F_{\max}^{\mathrm{ref}}$ reference fraction of the maximal tetanic force generated by the masticatory muscles that equals 1/3

$\mathbf{F}^{\mathbf{RMF}}$ resultant muscle force vector

JRF Joint reaction force

HDI highest density interval

L_{f} fiber length of a muscle at occlusion

L–T length-tension

$M_{\mathrm{x}}^{\mathrm{M}}, M_{\mathrm{y}}^{\mathrm{M}}, M_{\mathrm{z}}^{\mathrm{M}}$ moments about the X, Y, and Z axes of the masticatory muscles

PCSA Physiological cross-sectional area

pd probability of direction

$\mathbf{r}^{\mathbf{J_{bs}}}$ 3D position vector of the balancing-side TMJ

$\mathbf{r}^{\mathbf{M_{i,j}}}$ 3D position vector of the *j*-th segment of the *i*-th muscle

RMF Resultant muscle force

ROPE region of practical equivalence

TMJ Temporomandibular joint

ToS Triangle of support

α pennation angle of a muscle at occlusion

$\alpha_{(\mathrm{gape})}$ pennation angle of a muscle at a given gape angle

ε_{f} fiber strain, i.e., relative change in muscle fiber length, for a given gape with respect to occlusion

θ ToS plane angle, the angle between the ToS plane and the horizontal plane

ϕ resultant muscle force angle, the angle between the resultant muscle force vector and the coronal plane

$\Delta m_{(\text{gape})}$ difference in the length of the muscle-tendon unit (MTU) between occlusion and a given gape angle

ΔL_{occ} occlusal offset length, the difference in normalized fiber length between occlusion and when maximum force is generated in the length-tension curve

ACKNOWLEDGEMENTS

The 3D models of ancient Nubian mandibles are from the Semna South site, Sudan, housed in the School of Human Evolution and Social Change at Arizona State University. Scanning was conducted as part of NSF grants BCS-1551766 (to Claire Terhune), BCS-1551669 (to Siobhan Cooke), and BCS-1551722 (to Claire Kirchhoff). These models are used with permission of Dr. Claire Terhune and Dr. Brenda J. Baker, Curator of Nubian Collections at ASU. We thank Callum Ross, Kaleb Sellers, and two anonymous reviewers for helpful comments on the manuscript.

Funding

This project was funded by the Appalachian College Association (Semester Professional Leave Fellowship to J.I.D).

Data and resource availability

All relevant data can be found within the article and its supplementary information. MATLAB code and examples are available at https://github.com/jiriarte-sewanee/Triangle-of-support_JEB.

Competing interests

The authors declare no competing or financial interests.

REFERENCES

Agostinelli, C. and Lund, U. (2024). R package "circular": Circular Statistics (version 0.5-1).

Armfield, B. A. and Vinyard, C. J. (2010). An interspecific analysis of relative jaw-joint height in primates. *Am J Phys Anthropol* **142**, 519–530. https://doi.org/10.1002/ajpa.21251

Arnold, C., Matthews, L. J. and Nunn, C. L. (2010). The 10kTrees website: A new online resource for primate phylogeny. *Evol Anthropol* **19**, 114–118. https://doi.org/10.1002/evan.20251

Bürkner, P. C. (2018). Advanced Bayesian multilevel modeling with the R package brms. *R Journal* **10**, 395–411. https://doi.org/10.32614/RJ-2018-017

Clausen, P., Wroe, S., McHenry, C., Moreno, K. and Bourke, J. (2008). The vector of jaw muscle force as determined by computer-generated three dimensional simulation: A test of Greaves' model. *J Biomech* **41**, 3184–3188. https://doi.org/10.1016/j.jbiomech.2008.08.019

Coiner-Collier, S., Scott, R. S., Chalk-Wilayto, J., Cheyne, S. M., Constantino, P., Dominy, N. J., Elgart, A. A., Glowacka, H., Loyola, L. C., Ossi-Lupo, K., et al. (2016). Primate dietary ecology in the context of food mechanical properties. *J Hum Evol* **98**, 103–118. https://doi.org/10.1016/j.jhevol.2016.07.005

Constantino, P. J. (2007). Primate masticatory adaptations to fracture-resistant foods. *PhD Thesis*, George Washington University, Washington, DC.

Cook, R. W., Vazzana, A., Sorrentino, R., Benazzi, S., Smith, A. L., Strait, D. S. and Ledogar, J. A. (2021). The cranial biomechanics and feeding performance of *Homo floresiensis*. *Interface Focus* **11**, 20200083. https://doi.org/10.1098/rsfs.2020.0083

Crompton, A. W., Lieberman, D. E. and Aboelela, S. (2006). Tooth orientation during occlusion and the functional significance of condylar translation in primates and herbivores. In *Amniote Paleobiology: Perspectives on the Evolution of Mammals, Birds and Reptiles*. (ed. Carrano, M. T.), Gaudin, T. J.), Blob, R. W.), and Wi, J. R.), pp. 367–388. Chicago: University of Chicago Press.

Dickinson, E., Basham, C., Rana, A. and Hartstone-Rose, A. (2019). Visualization and quantification of digitally dissected muscle fascicles in the masticatory muscles of *Callithrix jacchus* using nondestructive DiceCT. *Anat Rec* **302**, 1891–1900. https://doi.org/10.1002/ar.24212

Fedorov, A., Beichel, R., Kalpathy-Cramer, J., Finet, J., Fillion-Robin, J. C., Pujol, S., Bauer, C., Jennings, D., Fennessy, F., Sonka, M., et al. (2012). 3D Slicer as an image computing platform for the Quantitative Imaging Network. *Magn Reson Imaging* **30**, 1323–1341. https://doi.org/10.1016/j.mri.2012.05.001

Fricano, E. E. I. and Perry, J. M. G. (2019). Maximum bony gape in primates. *Anat Rec* **302**, 215–225. https://doi.org/10.1002/ar.23897

Glowacka, H. and Schwartz, G. T. (2021). A biomechanical perspective on molar emergence and primate life history. *Sci Adv* **7**, eabj0335. https://doi.org/10.1126/sciadv.abj0335

Gordon, A. M., Huxley, A. F. and Julian, F. J. (1966). The variation in isometric tension with sarcomere length in vertebrate muscle fibres. *J Physiol* **184**, 170–192. https://doi.org/10.1113/jphysiol.1966.sp007909

Grant, P. G. (1973). Lateral pterygoid: Two muscles? *Am J Anat* **138**, 1–9. https://doi.org/10.1002/aja.1001380102

Greaves, W. S. (1978). The jaw lever system in ungulates: a new model. *J Zool* **184**, 271–285. https://doi.org/10.1111/j.1469-7998.1978.tb03282.x

Greaves, W. S. (2012). *The mammalian jaw: A mechanical analysis*. Cambridge University Press.

Herring, S. W. and Herring, S. E. (1974). The superficial masseter and gape in mammals. *Am Nat* **108**, 561–576. https://doi.org/10.1086/282934

Herring, S. W. and Liu, Z. J. (2001). Loading of the temporomandibular joint: anatomical and *in vivo* evidence from the bones. *Cells Tissues Organs* **169**, 193–200. https://doi.org/10.1159/000047882

Hiraba, K., Hibino, K., Hiranuma, K. and Negoro, T. (2000). EMG activities of two heads of the human lateral pterygoid muscle in relation to mandibular condyle movement and biting force. *J Neurophysiol* **83**, 2120–2137. https://doi.org/10.1152/jn.2000.83.4.2120

Hogue, A. S. (2004). On the relation between craniodental form and diet in mammals: Marsupials as a Natural Experiment. *PhD Thesis*, Northwestern University, Evanston, IL.

Holmes, M. and Taylor, A. B. (2021). The influence of jaw-muscle fibre-type phenotypes on estimating maximum muscle and bite forces in primates. *Interface Focus* **11**, 20210009. https://doi.org/10.1098/rsfs.2021.0009

Huxley, A. F. and Niedergerke, R. (1954). Structural changes in muscle during contraction: Interference Microscopy of living muscle fibres. *Nature* **173**, 971–973. https://doi.org/10.1038/173971a0

Hylander, W. L. (1975). The human mandible: Lever or link? *Am J Phys Anthropol* **43**, 227–242. https://doi.org/10.1002/ajpa.1330430209

Hylander, W. L. (2013). Functional links between canine height and jaw gape in catarrhines with special reference to early hominins. *Am J Phys Anthropol* **150**, 247–259. https://doi.org/10.1002/ajpa.22195

Hylander, W. L., Ravosa, M. J., Ross, C. F., Wall, C. E. and Johnson, K. R. (2000). Symphyseal fusion and jaw-adductor muscle force: an EMG study. *Am J Phys Anthropol* **112**, 469–492. https://doi.org/10.1002/1096-8644(200008)112:4%3C469::AID-AJPA5%3E3.0.CO;2-V

Iriarte-Diaz, J., Terhune, C. E., Taylor, A. B. and Ross, C. F. (2017). Functional correlates of the position of the axis of rotation of the mandible during chewing in non-human primates. *Zoology* **124**, 106–118. https://doi.org/10.1016/j.zool.2017.08.006

Kruschke, J. K. and Liddell, T. M. (2018). The Bayesian new statistics: Hypothesis testing, estimation, meta-analysis, and power analysis from a Bayesian perspective. *Psychon Bull Rev* **25**, 178–206. https://doi.org/10.3758/s13423-016-1221-4

Laird, M. F., Iriarte-Diaz, J., Byron, C. D., Granatosky, M. C., Taylor, A. B. and Ross, C. F. (2023a). Gape drives regional variation in temporalis architectural dynamics in tufted capuchins. *Phil Trans R Soc B* **378**, 20220550. https://doi.org/10.1098/rstb.2022.0550

Laird, M. F., Kanno, C. M., Yoakum, C. B., Fogaça, M. D., Taylor, A. B., Ross, C. F., Chalk-Wilayto, J., Holmes, M. A., Terhune, C. E. and de Oliveira, J. A. (2023b). Ontogenetic changes in bite force and gape in tufted capuchins. *J Exp Biol* **226**, jeb245972. https://doi.org/10.1242/jeb.245972

Laird, M. F., Polvadore, T. A., Hirschkorn, G. A., McKinney, J. C., Ross, C. F., Taylor, A. B., Terhune, C. E. and Iriarte-Diaz, J. (2024). Tradeoffs between bite force and gape in *Eulemur* and *Varecia*. *J Morphol* **285**, e21699. https://doi.org/10.1002/jmor.21699

Ledogar, J. A., Smith, A. L., Benazzi, S., Weber, G. W., Spencer, M. A., Carlson, K. B., McNulty, K. P., Dechow, P. C., Grosse, I. R., Ross, C. F., et al. (2016a). Mechanical evidence that *Australopithecus sediba* was limited in its ability to eat hard foods. *Nat Commun* **7**, 10596. https://doi.org/10.1038/ncomms10596

Ledogar, J. A., Dechow, P. C., Wang, Q., Gharpure, P. H., Gordon, A. D., Baab, K. L., Smith, A. L., Weber, G. W., Grosse, I. R., Ross, C. F., et al. (2016b). Human feeding biomechanics: Performance, variation, and functional constraints. *PeerJ* **4**, e2242. https://doi.org/10.7717/peerj.2242

Ledogar, J. A., Benazzi, S., Smith, A. L., Dechow, P. C., Wang, Q., Cook, R. W., Neaux, D., Ross, C. F., Grosse, I. R., Wright, B. W., et al. (2025). Bite force production and the origin of *Homo*. *R Soc Open Sci* **12**, 241879. https://doi.org/10.7717/peerj.2242

Lenth, R. (2025). emmeans: Estimated marginal means, aka least-squares means. R package version 1.11.0-003.

Lucas, P. W. (2004). *Dental functional morphology: how teeth work*. Cambridge University Press.

Lüdecke, D., Ben-Shachar, M., Patil, I., Waggoner, P. and Makowski, D. (2021). performance: An r package for assessment, comparison and testing of statistical models. *J Open Source Softw* **6**, 3139. https://doi.org/10.21105/joss.03139

Makowski, D., Ben-Shachar, M. S. and Lüdecke, D. (2019a). bayestestR: Describing effects and their uncertainty, existence and significance within the Bayesian framework. *J Open Source Softw* **4**, 1541. https://doi.org/10.21105/joss.01541

Makowski, D., Ben-Shachar, M. S., Chen, S. H. A. and Lüdecke, D. (2019b). Indices of effect existence and significance in the Bayesian framework. *Front Psychol* **10**, 2767. https://doi.org/10.3389/fpsyg.2019.02767

McNamara, J. A. (1973). The independent functions of the two heads of the lateral pterygoid muscle. *Am J Anat* **138**, 197–205. https://doi.org/10.1002/aja.1001380206

Mitchell, D. R. (2019). The anatomy of a crushing bite: The specialised cranial mechanics of a giant extinct kangaroo. *PLoS One* **14**, e0221287. https://doi.org/10.1371/journal.pone.0221287

Murray, G. M. (2012). The lateral pterygoid muscle: function and dysfunction. *Semin Orthod* **18**, 44–50. https://doi.org/10.1053/j.sodo.2011.10.001

Murray, G. M., Bhutada, M., Peck, C. C., Phanachet, I., Sae-Lee, D. and Whittle, T. (2007). The human lateral pterygoid muscle. *Arch Oral Biol* **52**, 377–380. https://doi.org/10.1016/j.archoralbio.2006.10.002

Perry, J. M. G. (2008). The anatomy of mastication in extant strepsirrhines and Eocene adapines. *PhD Thesis*, Duke University, NC.

Perry, J. M. G. and Hartstone-Rose, A. (2010). Maximum ingested food size in captive strepsirrhine primates: Scaling and the effects of diet. *Am J Phys Anthropol* **142**, 625–635. https://doi.org/10.1002/ajpa.21285

Powell, P. L., Roy, R. R., Kanim, P., Bello, M. A. and Edgerton, V. R. (1984). Predictability of skeletal muscle tension from architectural determinations in guinea pig hindlimbs. *J Appl Physiol* **57**, 1715–1721. https://doi.org/10.1152/jappl.1984.57.6.1715

R Core Team (2024). R: A Language and Environment for Statistical Computing.

Ravosa, M. J. and Vinyard, C. J. (2020). Masticatory loading and ossification of the mandibular symphysis during anthropoid origins. *Sci Rep* **10**, 5950. https://doi.org/10.1038/s41598-020-62025-8

Ravosa, M. J., Vinyard, C. J., Gagnon, M. and Islam, S. A. (2000). Evolution of anthropoid jaw loading and kinematic patterns. *Am J Phys Anthropol* **112**, 493–516. https://doi.org/10.1002/1096-8644(200008)112:4%3C493::AID-AJPA6%3E3.0.CO;2-P

Reed, D. A., Iriarte-Diaz, J. and Diekwisch, T. G. H. (2016). A three dimensional free body analysis describing variation in the musculoskeletal configuration of the cynodont lower jaw. *Evol Dev* **18**, 41–53. https://doi.org/10.1111/ede.12171

Ross, C. F. and Iriarte-Diaz, J. (2014). What does feeding system morphology tell us about feeding? *Evol Anthropol* **23**, 105–120. https://doi.org/10.1002/evan.21410

Ross, C. F., Iriarte-Diaz, J. and Nunn, C. L. (2012). Innovative approaches to the relationship between diet and mandibular morphology in primates. *Int J Primatol* **33**, 632–660. https://doi.org/10.1007/s10764-012-9599-y

Santana, S. E. (2016). Quantifying the effect of gape and morphology on bite force: biomechanical modelling and in vivo measurements in bats. *Funct Ecol* **30**, 557–565. https://doi.org/10.1111/1365-2435.12522

Santana, S. E., Grossnickle, D. M., Sadier, A., Patterson, E. and Sears, K. E. (2022). Bat dentitions: a model system for studies at the interface of development, biomechanics, and evolution. *Integr Comp Biol* **62**, 762–773. https://doi.org/10.1093/icb/icac042

Scott, J. E., Hogue, A. S. and Ravosa, M. J. (2012). The adaptive significance of mandibular symphyseal fusion in mammals. *J Evol Biol* **25**, 661–673. https://doi.org/10.1111/j.1420-9101.2012.02457.x

Singleton, M. (2015). Functional geometric morphometric analysis of masticatory system ontogeny in papionin primates. *Anat Rec* **298**, 48–63. https://doi.org/10.1002/ar.23068

Smith, R. J. (1978). Mandibular biomechanics and temporomandibular joint function in primates. *Am J Phys Anthropol* **49**, 341–349. https://doi.org/10.1002/ajpa.1330490307

Smith, A. L., Benazzi, S., Ledogar, J. A., Tamvada, K., Pryor Smith, L. C., Weber, G. W., Spencer, M. A., Lucas, P. W., Michael, S., Shekeban, A., et al. (2015). The feeding biomechanics and dietary ecology of *Paranthropus boisei*. *Anat Rec* **298**, 145–167. https://doi.org/10.1002/ar.23073

Spencer, M. A. (1995). Masticatory system configuration and diet in anthropoid primates. *PhD Thesis*, State University of New York at Stony Brook, Stony Brook, NY.

Spencer, M. A. (1998). Force production in the primate masticatory system: electromyographic tests of biomechanical hypotheses. *J Hum Evol* **34**, 25–54. https://doi.org/10.1006/jhev.1997.0180

Spencer, M. a. (1999). Constraints on masticatory system evolution in anthropoid primates. *Am J Phys Anthropol* **108**, 483–506. https://doi.org/10.1002/(SICI)1096-8644(199904)108:4%3C483::AID-AJPA7%3E3.0.CO;2-L

Strait, S. G. (1997). Tooth use and the physical properties of food. *Evol Anthropol* **5**, 199–211. https://doi.org/10.1002/(SICI)1520-6505(1997)5:6%3C199::AID-EVAN2%3E3.0.CO;2-8

Taylor, A. B. (2002). Masticatory form and function in the african apes. *Am J Phys Anthropol* **117**, 133–156. https://doi.org/10.1002/ajpa.10013

Taylor, A. B. and Vinyard, C. J. (2013). The relationships among jaw-muscle fiber architecture, jaw morphology, and feeding behavior in extant apes and modern humans. *Am J Phys Anthropol* **151**, 120–134. https://doi.org/10.1002/ajpa.22260

Taylor, A. B., Holmes, M. A., Laird, M. F. and Terhune, C. E. (2025). Jaw-muscle structure and function in primates: Insights into muscle performance and feeding-system behaviors. *Evol Anthropol* **34**, e22053. https://doi.org/10.1002/evan.22053

Terhune, C. E. (2011). Modeling the biomechanics of articular eminence function in anthropoid primates. *J Anat* **219**, 551–564. https://doi.org/10.1111/j.1469-7580.2011.01424.x

Terhune, C. E., Cooke, S. B. and Otárola-Castillo, E. (2015). Form and function in the platyrrhine skull: a three-dimensional analysis of dental and TMJ morphology. *Anat Rec* **298**, 29–47. https://doi.org/10.1002/ar.23062

Terhune, C. E., Mitchell, D. R., Cooke, S. B., Kirchhoff, C. A. and Massey, J. S. (2022). Temporomandibular joint shape in anthropoid primates varies widely and is patterned by size and phylogeny. *Anat Rec* **305**, 2227–2248. https://doi.org/10.1002/ar.24886

Vinyard, C. J., Wall, C. E., Williams, S. H., Mork, A. L., Armfield, B. A., Melo, L. C. de O., Valença-Montenegro, M. M., Valle, Y. B. M., de Oliveira, M. A. B., Lucas, P. W., et al. (2009). The Evolutionary Morphology of Tree Gouging in Marmosets. In *The smallest anthropoids* (ed. S. Ford, L. Porter and L. Davis), pp. 395–409. Boston, MA: Springer. https://doi.org/10.1007/978-1-4419-0293-1_20

Wheelwright, N. T. (1985). Fruit-size, gape width, and the diets of fruit-eating birds. *Ecology* **66**, 808–818. https://doi.org/10.2307/1940542

Wilken, A. T., Schultz, J. A., Luo, Z.-X. and Ross, C. F. (2024). A new biomechanical model of the mammal jaw based on load path analysis. *J Exp Biol* **227**, jeb247030. https://doi.org/10.1242/jeb.247030

Wright, B. (2005). Craniodental biomechanics and dietary toughness in the genus *Cebus*. *J Hum Evol* **48**, 473–492. https://doi.org/10.1016/j.jhevol.2005.01.006

Yamashita, N., Vinyard, C. J. and Tan, C. L. (2009). Food mechanical properties in three sympatric species of *Hapalemur* in Ranomafana National Park, Madagascar. *Am J Phys Anthropol* **139**, 368–381. https://doi.org/10.1002/ajpa.20992

Zajac, F. E. (1989). Muscle and tendon: properties, models, scaling, and application to biomechanics and motor control. *Crit Rev Biomed Eng* **17**, 359–410.

Figures

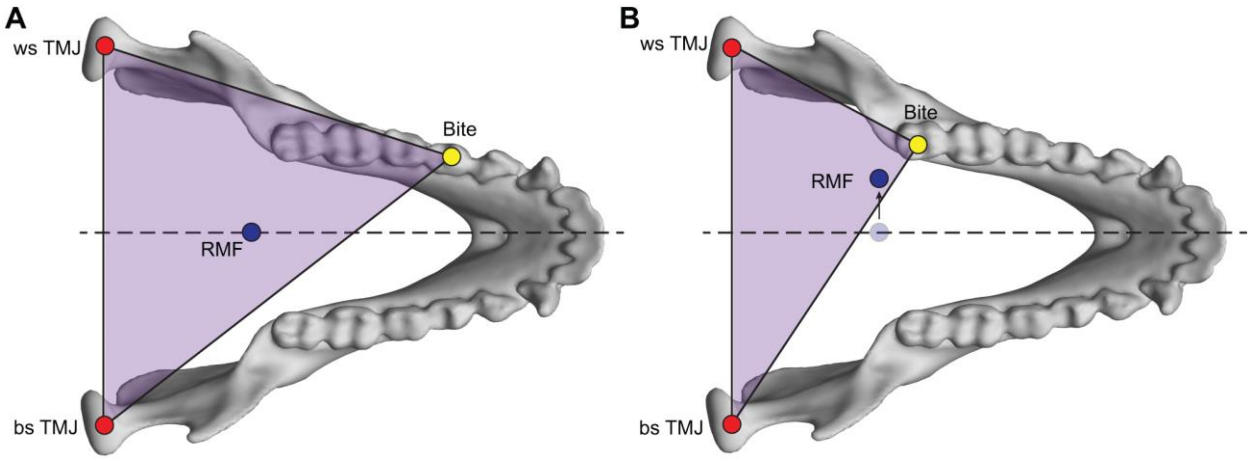

Fig. 1. Predictions of the constrained lever model. (A) For anterior bites, the resultant muscle force (RMF), which is in the midline (dashed line) when the adductor muscles are fully activated, is located inside the triangle of support (ToS, purple triangle). The vertices of the ToS are defined by the working- and balancing-side TMJs (red circles), and the bite point (yellow circle). When the RMF is inside the ToS, both TMJs experience compressive forces. **(B)** For posterior bites, the RMF might fall outside of the ToS, which is predicted to generate distracting forces on the working-side (ws) TMJ. To prevent this, the RMF is expected to shift towards the working side by reducing the forces generated by balancing-side muscles.

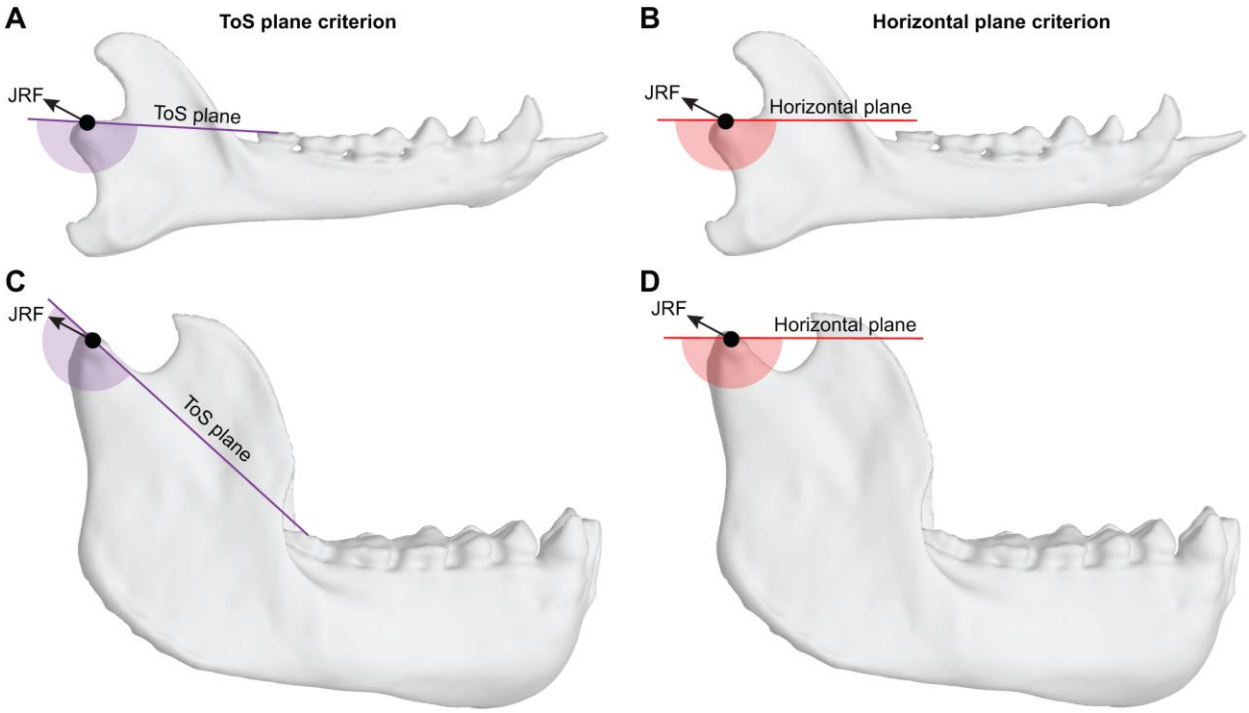

Fig. 2. Effect of TMJ height on the determination of distracting joint forces. The black arrows represent the same hypothetical joint reaction force (JRF) vector acting on the jaw joints of a lemur (*Lemur catta*, **A**,**B**) and gorilla (*Gorilla gorilla*, **C,D**). Using the ToS plane criterion from the CLM (**A,C**), the JRF is above the ToS plane in the lemur and considered compressive (non-distractive), but the same JRF is considered distractive in the gorilla (within the purple semicircle). This mismatch results from differences in the height of the TMJ and orientation of the ToS plane in these taxa. Using a constant plane, here a horizontal plane criterion (**B,D**), the JRF would be considered compressive (non-distracting) in both species (JRF is above the red semicircle).

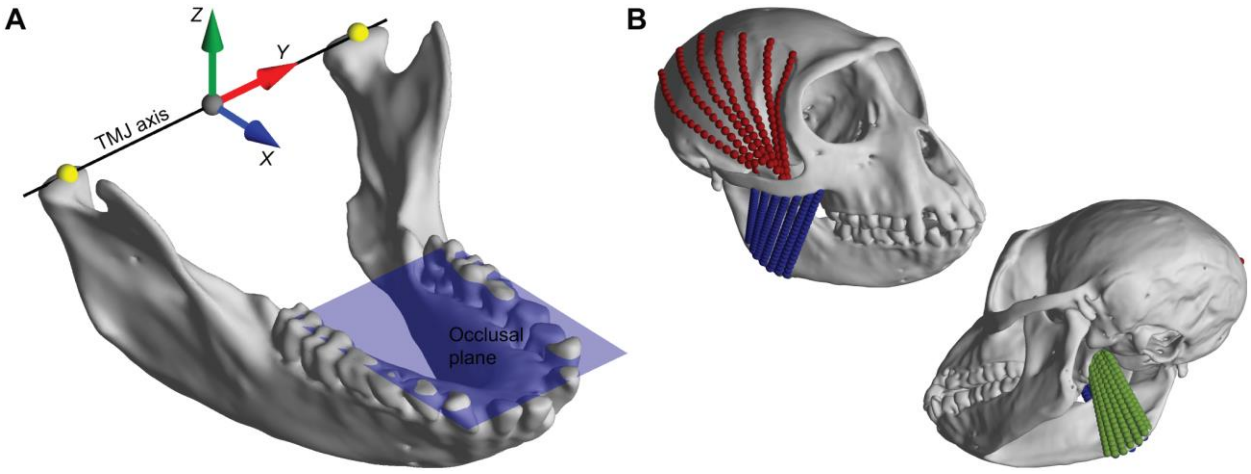

Fig. 3. Model preparation. (A) Coordinate system used to orient the cranium and mandible models. The *Y*-axis is aligned to the TMJ axis, the axis that connects the two temporomandibular joints (TMJs, yellow circles). The occlusal plane is parallel to the *X*–*Y* plane. The origin (gray circle) is located at the midpoint between the two TMJs **(B).** Example of the virtual jaw adductor muscles (blue, superficial masseter; red, temporalis; green, medial pterygoid) mapped onto the cranium and mandible of an Allen's swamp monkey (*Allenopithecus negroviridis*). Each muscle was modeled as seven independent muscle segments.

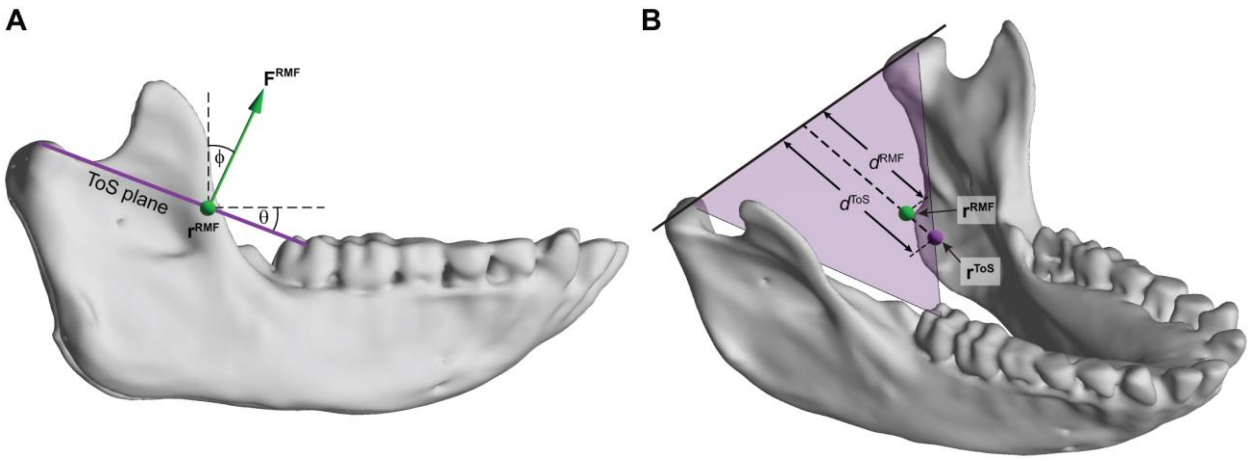

Fig. 4. Position of the resultant muscle force (RMF). (A) Lateral view of a mandible of a female Allen's swamp monkey (*Allenopithecus negroviridis*) showing the RMF vector, $\mathbf{F}^{\mathbf{RMF}}$ (green arrow). The point where this vector intersects the ToS plane (purple line) is the $\mathbf{r}^{\mathbf{RMF}}$. The angle between the ToS plane and the horizontal plane is the ToS plane angle, θ, and the angle between the $\mathbf{F}^{\mathbf{RMF}}$ and the vertical is the RMF angle, ϕ. **(B)** Metrics used to describe the relative position of the RMF. d^{RMF} and d^{ToS} are the perpendicular distances of the RMF position ($\mathbf{r}^{\mathbf{RMF}}$) and the anterior edge of the ToS ($\mathbf{r}^{\mathbf{ToS}}$) to the TMJ axis, respectively.

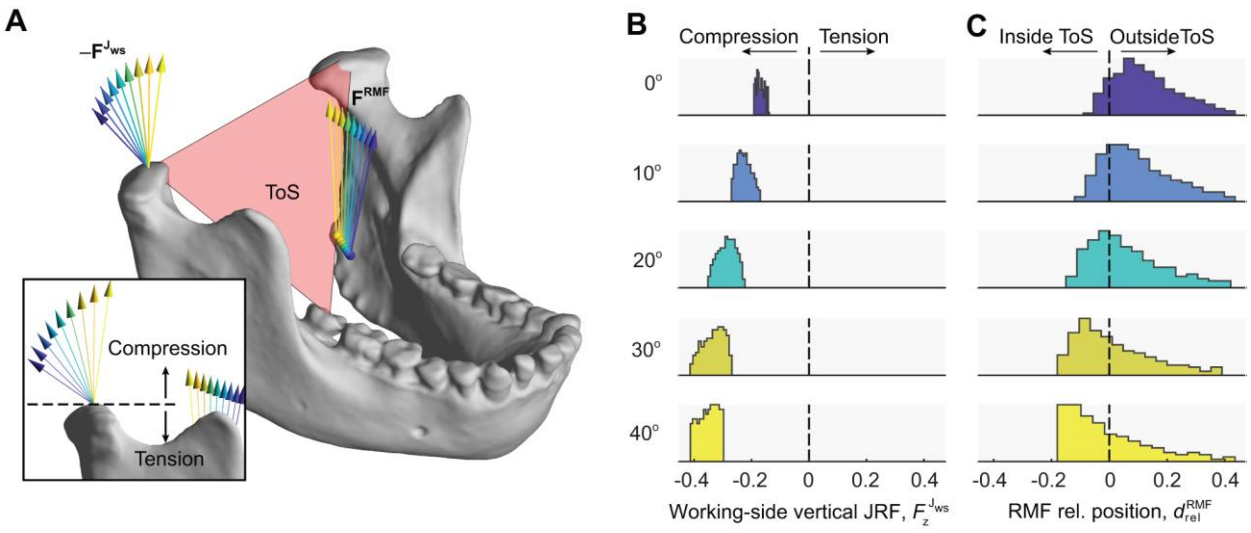

Fig. 5. Forces at the working-side TMJ and the position of RMFs in *Pan paniscus* at different gape angles. (A) Diagram showing the RMF vectors ($\mathbf{F}^{\mathbf{RMF}}$) relative to the triangle of support (ToS, red area) and the inverse of joint reaction forces (JRFs) vectors acting on the working-side TMJ ($-\mathbf{F}^{\mathbf{J_{WS}}}$). The direction of the JRFs was inverted for clarity, so that the arrows do not converge on the joint. The color of the vector represents a different gape angle from 0° (dark blue) to 40° (yellow). The inset depicts the JRFs from a lateral view, showing that for every gape angle, the working-side TMJ exhibits compressive forces. **(B, C)** Histograms showing the distribution of the relative muscle force effect on the working-side vertical JRF and the RMF position relative to the ToS for different gape angles. For the JRFs, negative values indicate that the forces are compressive, pushing the mandibular condyle towards the cranium, and maintaining the stability of the joint. For the RMF position, negative values indicate that the RMF is located inside the ToS, while positive values indicate that the RMF is outside the ToS.

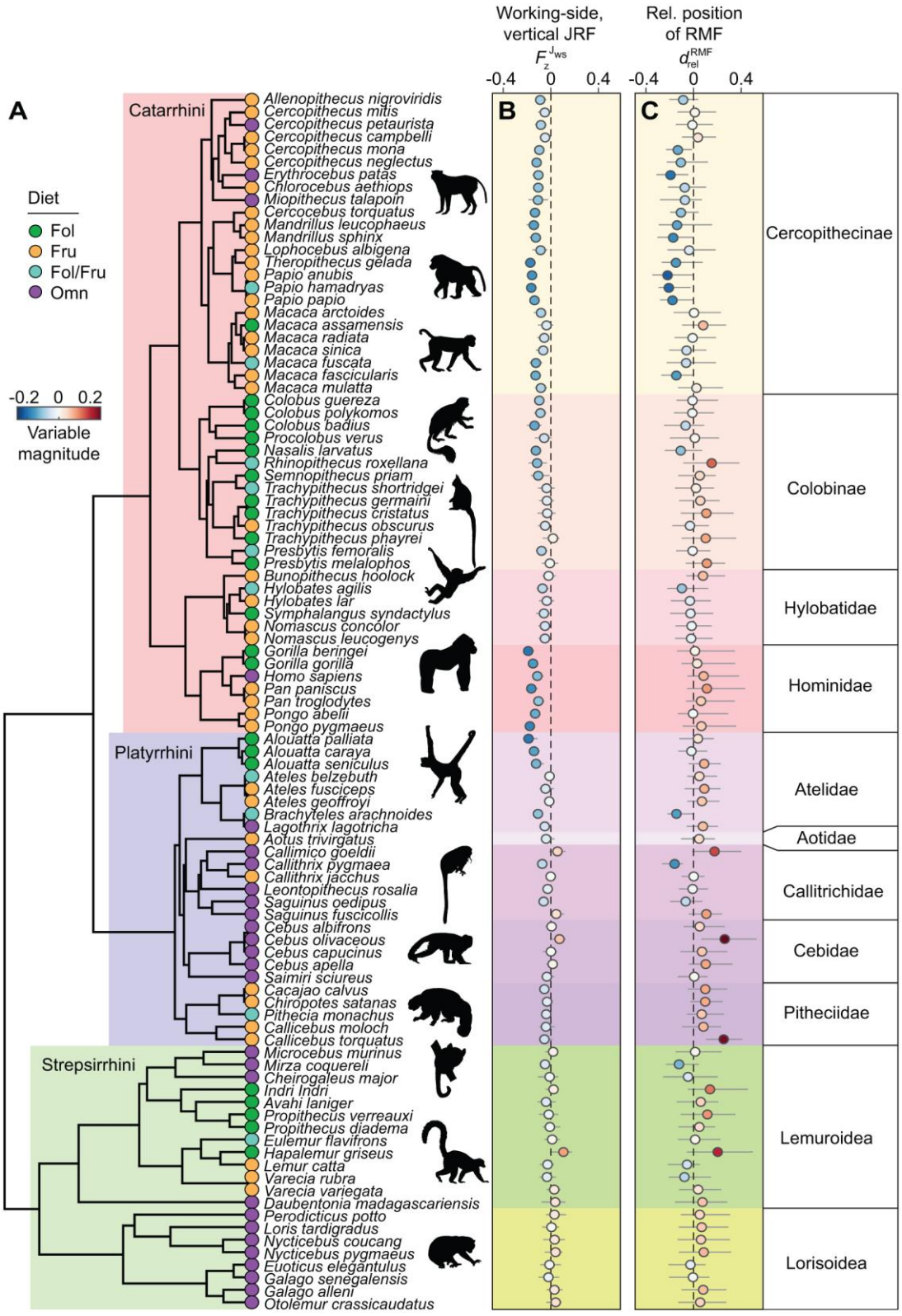

Fig. 6. Working-side vertical JRF and relative position of the RMF at occlusion across primates. **(A)** Phylogenetic relationship and dietary categories (Fol=folivore, Fru=frugivore, Fol/Fru=folivore/frugivore, Omn=omnivore) of the 97 species in this study. Colored boxes around the phylogeny indicate species that belong to the infraorder catarrhini, the infraorder platyrrhini, and the suborder strepsirrhini. **(B)** Working-side, vertical JRF (F_z^{Jws}) at 0° gape. Positive values indicate that the forces are distracting forces. Symbols and error bars represent the median value and range of the distribution of the relative muscle force effect. Symbols are color-coded according to the magnitude of the variable. Background colors represent either the family or the subfamily. **(C)** Relative position of the RMF with respect to the ToS ($d_{\mathrm{rel}}^{\mathrm{RMF}}$). Positive values indicate that the RMF is located outside the ToS. All primate silhouettes are from PhyloPic (www.phylopic.org).

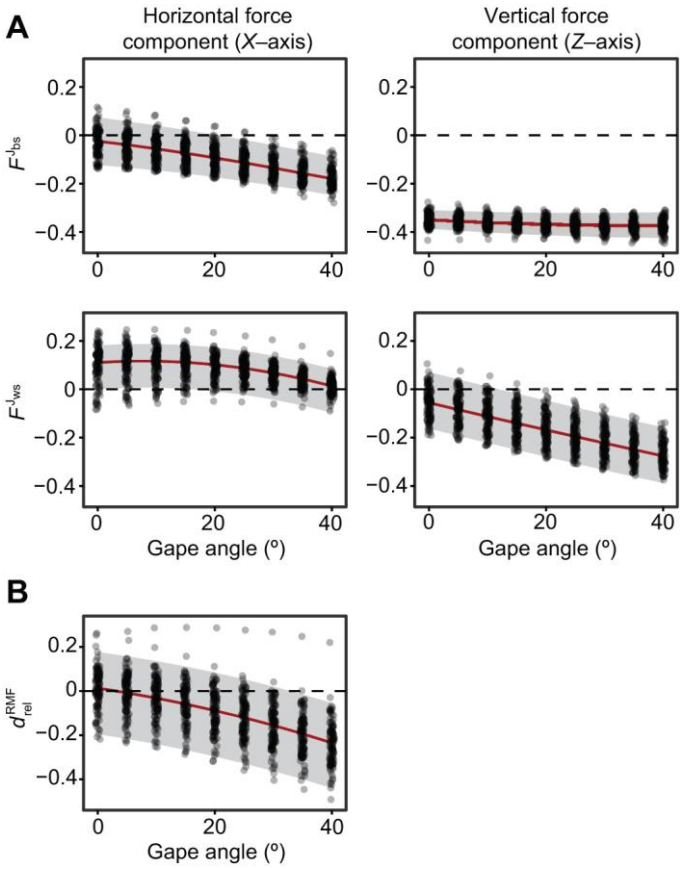

Fig. 7. Effect of gape on JRFs and the position of the RMF. (A) Relationship between JRFs and gape angle. The left panels represent the horizontal (antero-posterior) JRF components. The right panels show the vertical JRF components, where positive values indicate tensile/distracting forces. **(B)** Relationship between the relative position of the RMF and gape angle. Positive values indicate that the RMF vector is located outside the ToS. Red line and gray shaded areas represent the Bayesian regression fit and 95% credible intervals.

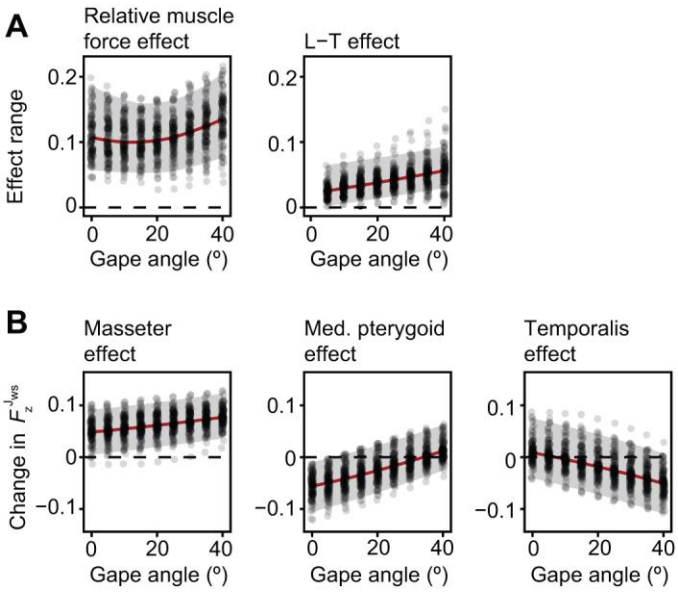

Fig. 8. Effect of gape angle on the variables that can affect the working-side joint reaction force. (A) Relationship between gape angle and the range of the relative muscle force and the L–T effects. **(B)** Relationship between gape angle and the effect of the masseter, medial pterygoid, and temporalis on the working-side JRF. The red lines represent the Bayesian regression fit, and the gray areas are their 95% credible intervals.

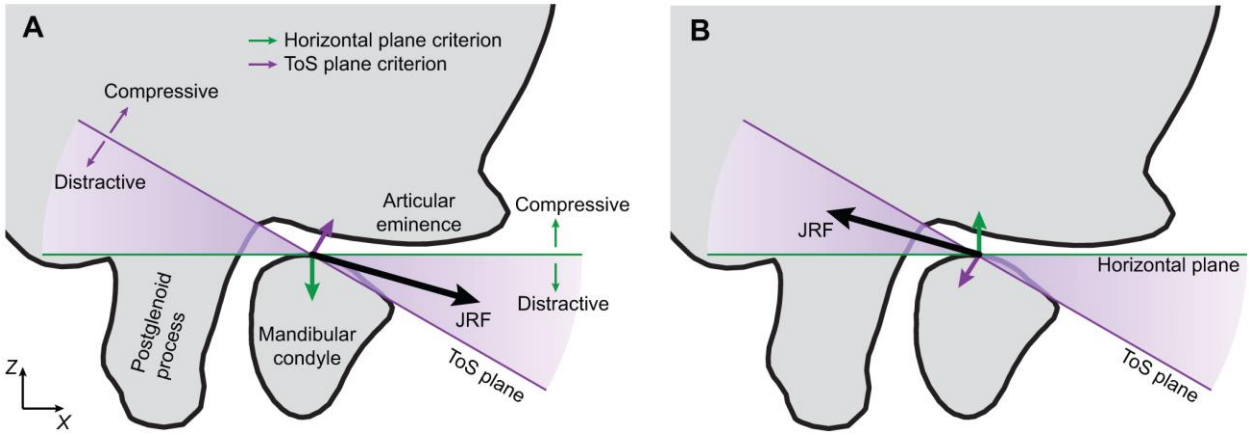

Fig. 9. Conditions where the two criteria of joint stability give contrasting results. Two sagittal sections through the TMJ that illustrate differences in the definition of distractive forces under the ToS plane criterion (thin purple arrows) and the horizontal plane criterion (thin green arrows). **(A)** If the joint reaction force (JRF, black arrow) lies above the ToS plane (purple line) but below the horizontal plane (green line), the component of the JRF perpendicular to the ToS plane (thick purple arrow) points towards the cranium, which based on the oblique ToS plane criterion, indicating that the joint is under compressive forces. However, under the horizontal plane, the JRF still has a vertical force component (thick green arrow) that pulls the mandible away from the cranium. **(B)** If the JRF lies below the ToS plane but above the horizontal plane, the JRF component perpendicular to the ToS plane (purple arrow) indicates that the joint experiences distracting forces, according to the oblique ToS plane criterion. However, under the horizontal plane criterion, the JRF still has a vertical force component that pushes the mandible upwards towards the cranium (green arrow).

Supplementary Material and Methods

Derivation of bite and joint reaction forces

We modeled the mechanics of the mandible as a rigid body with four external forces: a known muscle force ($\mathbf{F^M}$), a bite force ($\mathbf{F^B}$), and two joint reaction forces, $\mathbf{F^{Jws}}$ and $\mathbf{F^{Jbs}}$, acting at the working- and balancing-side temporomandibular joints (TMJs), respectively. To make calculations easier, we centered the system at the balancing-side TMJ, and oriented the models so that the *Y*-axis is aligned with the TMJ axis (the line connecting the two TMJs) and pointing towards the left side, and the *Z*-axis is perpendicular to the occlusal plane and pointing upwards (**Fig. S1**). Bolded terms indicate vectors and italicized terms indicate scalars.

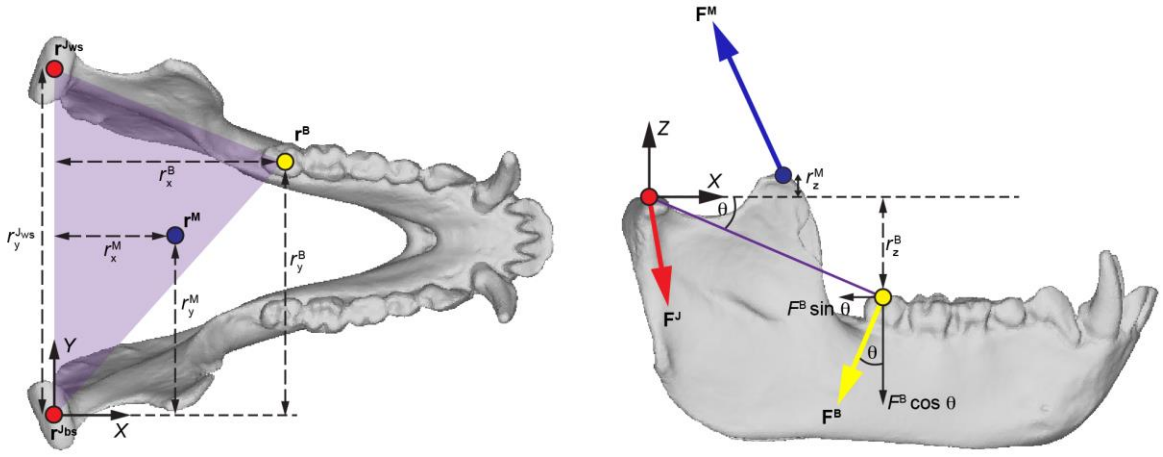

Fig. S1. Forces acting on the primate mandible. The red circles indicate the position of the working- and balancing-side TMJs and the yellow dot indicates the position of the bite point. The origin is located at the balancing-side TMJ. The resultant muscle force $\mathbf{F^M}$, in this case, representing the force generated by the temporalis, is applied at the muscle position vector $\mathbf{r^M}$. The muscle force is located in the midsagittal plane because the muscles on the left and right sides generate equal amounts of force. This force will create moments around the TMJ axis that will be balanced by the bite force $\mathbf{F^B}$ applied at the position vector $\mathbf{r^B}$, and by the working- and balancing-side joint reactions forces ($\mathbf{F^{Jws}}$ and $\mathbf{F^{Jbs}}$, respectively) applied at the position vectors $\mathbf{r^{Jws}}$ and $\mathbf{r^{Jbs}}$. The purple region indicates the triangle of support (ToS) and the angle θ indicates the ToS plane angle.

Assuming static equilibrium, the sum of all the forces and moments acting on the mandible must be equal to zero. The moments produced by the muscle force ($\mathbf{M^M}$) at the origin (i.e., the balancing-side TMJ) were calculated as:

$$\mathbf{M^M} = \begin{bmatrix} M_x^M \\ M_y^M \\ M_z^M \end{bmatrix} = \mathbf{r^M} \otimes \mathbf{F^M} \#(1)$$

where $\mathbf{r^M}$ is the position vector of the muscle force and $\otimes$ denotes a vector cross-product.

Thus, the equations describing the relationship can be written as:

$$\sum F_x = 0 = F_x^M + F_x^B + F_x^{Jws} + F_x^{Jbs} \#(2)$$

$$\sum F_y = 0 = F_y^M + F_y^B + F_y^{Jws} + F_y^{Jbs} \#(3)$$

$$\sum F_z = 0 = F_z^M + F_z^B + F_z^{Jws} + F_z^{Jbs} \#(4)$$

$$\sum M_x = 0 = M_x^M + M_x^B + M_x^{Jws} + M_x^{Jbs} \#(5)$$

$$\sum M_y = 0 = M_y^M + M_y^B + M_y^{Jws} + M_y^{Jbs} \#(6)$$

$$\sum M_z = 0 = M_z^M + M_z^B + M_z^{Jws} + M_z^{Jbs} \#(7)$$

Because there are more unknown variables than the six independent equilibrium equations, we need to make some assumptions to solve the system. First, the jaw adductor muscles on both sides of the skull are activated maximally, so that the resultant muscle force has no lateral (*Y*) force component and is located at the midsagittal plane. Second, the direction of the bite force vector is perpendicular to the plane of the triangle of support, defined by the two TMJs and the bite point. This results in the bite force vector to be defined as
$\mathbf{F^B} = \left[F_x^B, F_y^B, F_z^B\right] = [F^B \sin\theta, 0, F^B \cos\theta]$.

Equation 6 can be expanded with zeroed terms as per our assumptions as

$$\left(r_z^B F_x^B - r_x^B F_z^B\right) + \left(\cancel{r_z^{Jws}} F_x^{Jws} - \cancel{r_x^{Jws}} F_z^{Jws}\right) + \left(\cancel{r_z^{Jbs}} F_x^{Jbs} - \cancel{r_x^{Jbs}} F_z^{Jbs}\right) = -M_y^M$$

$$\left(r_z^B F^B \sin\theta - r_x^B F^B \cos\theta\right) = F^B\left(r_z^B \sin\theta - r_x^B \cos\theta\right) = -M_y^M$$

We can then solve the magnitude of the biting force F^B as:

$$F^B = \frac{-M_y^M}{r_z^B \sin\theta - r_x^B \cos\theta} \#(8)$$

Equation 5 can be expanded with zeroed terms as per our assumptions as

$$\left(r_{\mathrm{y}}^{\mathrm{B}}F_{\mathrm{z}}^{\mathrm{B}} - r_{\mathrm{z}}^{\mathrm{B}}\cancel{F_{\mathrm{y}}^{\mathrm{B}}}\right) + \left(r_{\mathrm{y}}^{\mathrm{Jws}}F_{\mathrm{z}}^{\mathrm{Jws}} - \cancel{r_{\mathrm{z}}^{\mathrm{Jws}}}F_{\mathrm{y}}^{\mathrm{Jws}}\right) + \left(\cancel{r_{\mathrm{y}}^{\mathrm{Jbs}}}\mathrm{F}_{\mathrm{z}}^{\mathrm{Jbs}} - \cancel{r_{\mathrm{z}}^{\mathrm{Jbs}}}\mathrm{F}_{\mathrm{y}}^{\mathrm{Jbs}}\right) = -M_{\mathrm{x}}^{\mathrm{M}}$$

$$\left(r_{\mathrm{y}}^{\mathrm{B}}F^{\mathrm{B}}\cos\theta\right) + \left(r_{\mathrm{y}}^{\mathrm{Jws}}F_{\mathrm{z}}^{\mathrm{Jws}}\right) = -M_{\mathrm{x}}^{\mathrm{M}}$$

We can then solve for $F_{\mathrm{z}}^{\mathrm{Jws}}$ as

$$F_{\mathrm{z}}^{\mathrm{Jws}} = \frac{-M_{\mathrm{x}}^{\mathrm{M}} - r_{\mathrm{y}}^{\mathrm{B}}F^{\mathrm{B}}\cos\theta}{r_{\mathrm{y}}^{\mathrm{Jws}}} \#(9)$$

Equation 7 can be rearranged and expanded with zeroed terms as per our assumptions as:

$$\left(r_{\mathrm{x}}^{\mathrm{B}}\cancel{F_{\mathrm{y}}^{\mathrm{B}}} - r_{\mathrm{y}}^{\mathrm{B}}F_{\mathrm{x}}^{\mathrm{B}}\right) + \left(\cancel{r_{\mathrm{x}}^{\mathrm{Jws}}}F_{\mathrm{y}}^{\mathrm{Jws}} - r_{\mathrm{y}}^{\mathrm{Jws}}F_{\mathrm{x}}^{\mathrm{Jws}}\right) + \left(\cancel{r_{\mathrm{x}}^{\mathrm{Jbs}}}F_{\mathrm{y}}^{\mathrm{Jbs}} - \cancel{r_{\mathrm{y}}^{\mathrm{Jbs}}}F_{\mathrm{x}}^{\mathrm{Jbs}}\right) = -M_{\mathrm{z}}^{\mathrm{M}}$$

$$\left(-r_{\mathrm{y}}^{\mathrm{B}}F^{\mathrm{B}}\sin\theta\right) + \left(-r_{\mathrm{y}}^{\mathrm{Jws}}F_{\mathrm{x}}^{\mathrm{Jws}}\right) = -M_{\mathrm{z}}^{\mathrm{M}}$$

We can solve for $F_{\mathrm{x}}^{\mathrm{Jws}}$ as

$$F_{\mathrm{x}}^{\mathrm{Jws}} = \frac{-M_{\mathrm{z}}^{\mathrm{M}} + r_{\mathrm{y}}^{\mathrm{B}}F^{\mathrm{B}}\sin\theta}{-r_{\mathrm{y}}^{\mathrm{Jws}}} = \frac{M_{\mathrm{z}}^{\mathrm{M}} - r_{\mathrm{y}}^{\mathrm{B}}F^{\mathrm{B}}\sin\theta}{r_{\mathrm{y}}^{\mathrm{Jws}}} \#(10)$$

And finally, we can solve the force components of the balancing-side reaction forces by replacing the known factors in **equations 2** and **4** as:

$$F_{\mathrm{x}}^{\mathrm{Jbs}} = -F_{\mathrm{x}}^{\mathrm{M}} - F^{\mathrm{B}}\sin\theta - F_{\mathrm{x}}^{\mathrm{Jws}}$$

$$F_{\mathrm{z}}^{\mathrm{Jbs}} = -F_{\mathrm{z}}^{\mathrm{M}} - F^{\mathrm{B}}\cos\theta - F_{\mathrm{z}}^{\mathrm{Jws}}$$

In our model, the *Y*–component of the joint reaction forces is undefined.

Supplementary Results

Effect of muscle segment number on joint reaction force estimates

To test whether the number of modeled muscle segments affected our joint reaction forces estimates, we modeled differences in vertical joint reaction force on the working side (F_z^{Jws}) for a single modeled muscle segment (Single Muscle effect), four modeled muscle segments (Reduced Muscle effect), and seven modeled muscle segments in three species (one per major clade; *Macaca mulatta*, *Ateles belzebuth*, *Avahi laniger*). For the Single Muscle effect, we used the middle segment (segment 4), while for the Reduced Muscle effect, we used the segments 1, 3, 5, and 7.

In each of the three species, varying the number of muscle segments had a much smaller effect than changing the modeled force of each jaw adductor muscle (Muscle Force effect) (**Fig. S2**). If the number of muscle segment is reduced from seven to one (Single Muscle segment), the JRF is slightly more negative (about 1-2 percent points). If the number of segments is reduced from seven to four (Reduced Muscle effect), there is little effect on the JRF.

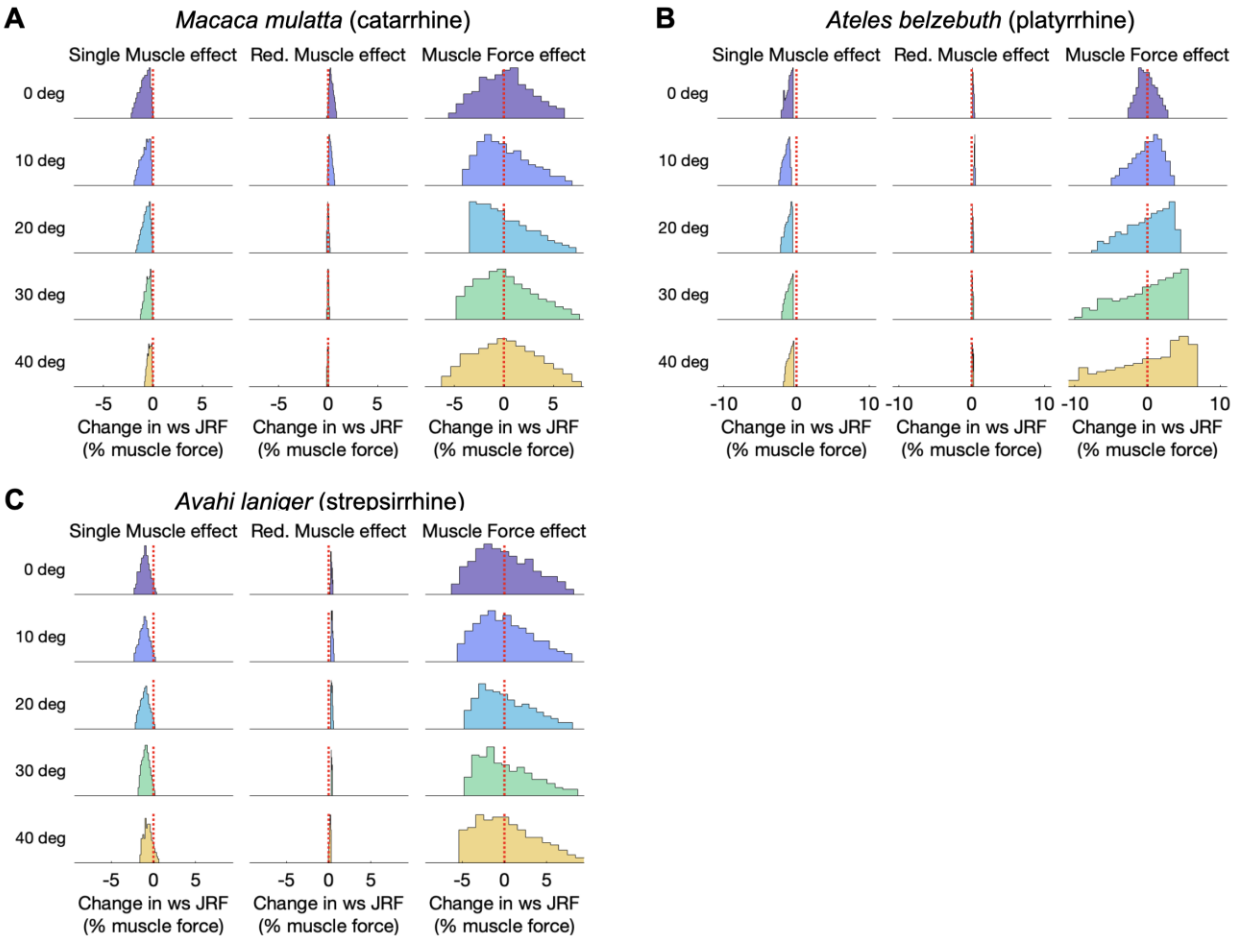

Fig. S2. Effect of muscle segment number on vertical working-side joint reaction force. For each species, the distribution of the effect on the joint reaction force of modeling each adductor muscle as a single muscle segment (Single Muscle effect, left panel) and of modeling each adductor muscle as four segments (Red. Muscle effect, middle panel). The right panel shows the effect of variation in the relative muscle force configuration on the vertical joint reaction force (same as in **Fig. S5A** below), to serve as a reference.

Validation of the model

Finite element analyses (FEA) were conducted on the mandibles of nine species, representing three from each major primate clade, to validate our mathematical model. Analyses were performed in MATLAB using the GIBBON toolbox (Moerman, 2018) for geometry processing and meshing, and FEBio v2.5 (Maas et al., 2012) for finite element simulations. The modeling pipeline began with the creation of tetrahedral meshes using TetGen (Si, 2015), integrated within the GIBBON toolbox. The mandible was modeled as cortical bone, assigned an isotropic elastic material with a Young's modulus (E) of 20 GPa and a Poisson's ratio (ν) of 0.3. As the

primary objective of this analysis was to estimate joint reaction forces rather than to evaluate strain and stress distribution patterns, teeth and trabecular bone were not modeled separately. Contact boundary conditions were defined by constraining translations at the three points of the triangle of support: the bite point was constrained in all directions, and the two temporomandibular joints (TMJs) were constrained in both the X-direction (antero-posterior displacement) and the Z-direction (infero-superior displacement). Muscle forces were applied at 42 points (3 muscles × 7 segments per muscle × 2 sides), with the positions and directions of the forces obtained directly from the virtual muscle segments used in the mathematical model. The total muscle force for each model was set to 100 N, yielding a force of 2.38 N per muscle segment (100 N divided by 42 segments), representing the reference muscle condition in which all three jaw adductor muscles generate equal force. A single muscle force was used for all models, regardless of body size differences, as the focus was on estimating relative joint reaction forces rather than absolute values. To model reaction forces at different gapes, the tetrahedral mesh was rotated using the same rotation matrix as in the mathematical model. From the solved FEA models at each gape, the 3D reaction forces at the bite point and the two TMJs were exported and normalized to the total muscle force.

Fig. S3 presents the comparison of joint reaction forces (JRFs) between the mathematical model (dotted lines) and the FE models (solid lines with symbols). The left panel displays the horizontal JRFs (F_x^J) for both the balancing-side (blue lines) and working-side joints (red lines), while the middle panel shows the vertical JRFs (F_z^J). The right panel shows the relationship between the angle of the bite force vector and gape angle. The solid black lines show the bite force angles from the FEA model; the dashed orange line shows the bite force angle used in this study, which assumes that the mandible functions as a lever and is perpendicular to the ToS plane; and the dotted yellow line shows the bite force angle if the mandible functions as a link, which is parallel to resultant muscle force (RMF).

This comparison indicates that although the correspondence is not exact, the relationship between joint reaction forces and gape follows a similar pattern in both the FE and mathematical models. Differences between the FEA and the mathematical model are more pronounced for the horizontal JRFs and the vertical balancing-side JRF. However, the vertical JRF, which is the primary focus of this study, shows stronger agreement. Some of the observed differences between the mathematical model and FEA likely stem from variations in the direction of the applied bite force. The mathematical model assumes the mandible functions as a lever, with the bite force oriented perpendicular to the triangle of support (ToS) plane

(Hylander, 1975). Alternatively, the mandible can be modeled as a link, with the bite force parallel to the resultant muscle force (RMF) vector (Hylander, 1975), or as a combination of both (Gingerich, 1979). To evaluate the significance of bite force direction, the bite force angle from the FEA was compared with both the ToS plane angle and the RMF angle. If the mandible acts as a lever, the FEA bite force angle should match the ToS plane angle; if it acts as a link, the angle should correspond to the RMF angle. The data indicate that, in most cases, the FEA bite angle falls between the ToS plane angle and the RMF angle but is generally closer to the ToS plane angle (**Fig. S3**, right panels). However, this pattern is not consistent across all species. For instance, in *Macaca*, *Callimico,* and *Nycticebus*, the FEA angle is closer to the RMF angle, whereas in *Saguinus*, *Avahi*, and *Hapalemur*, the ToS plane angle lies between the FEA and RMF angles. Given the inconsistency in bite force direction and the tendency for the FEA angle to approximate the ToS plane angle, the assumption that the bite force angle is perpendicular to the ToS plane appears justified.

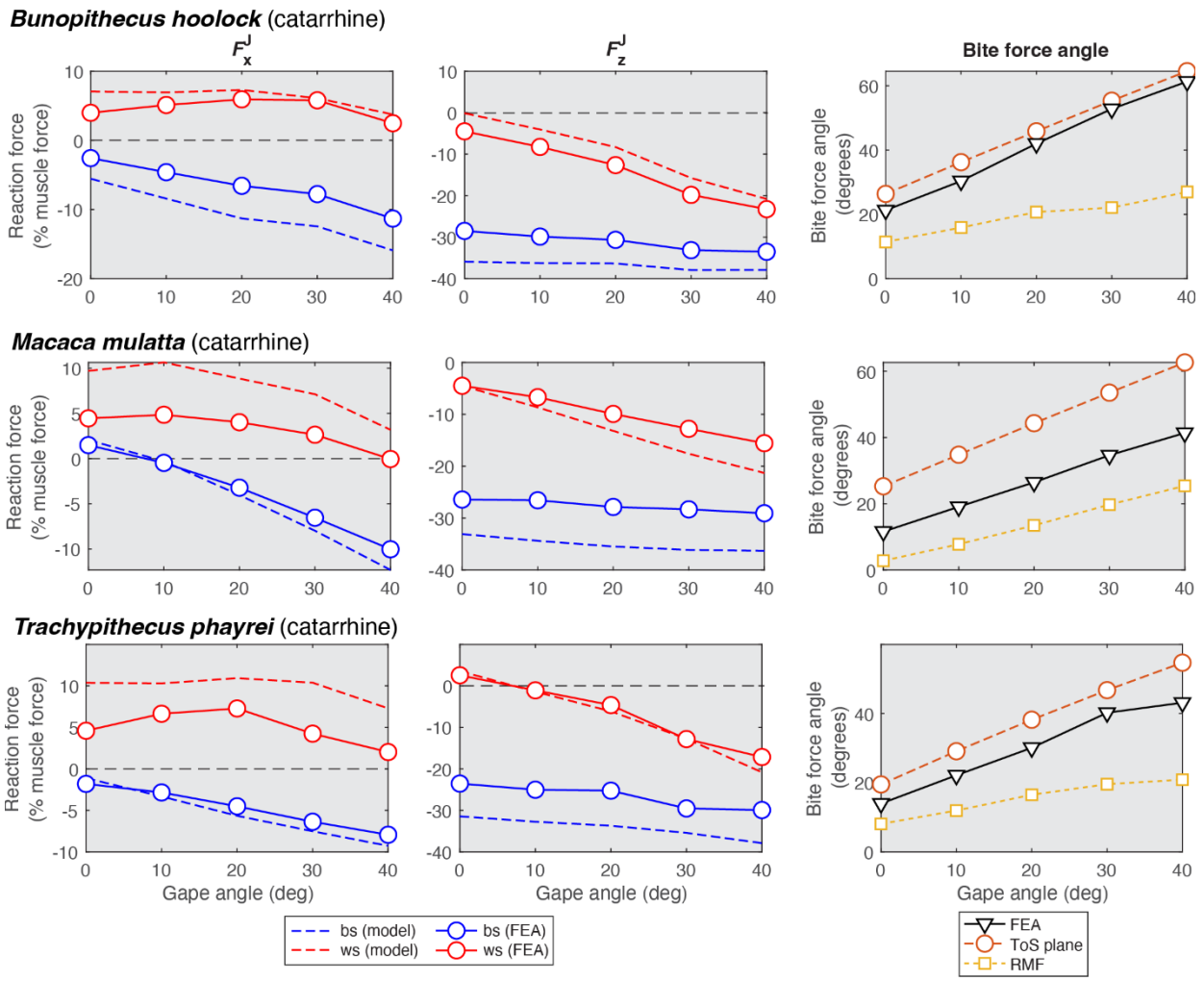

Fig. S3. Comparison between the mathematical and the FEA models. The left and middle panels depict the effect of gape on the horizontal (F_x^J) and vertical joint reaction forces (F_z^J), respectively. The right panel shows the effect of gape on the angle of different bite force vectors. See the text for more details.

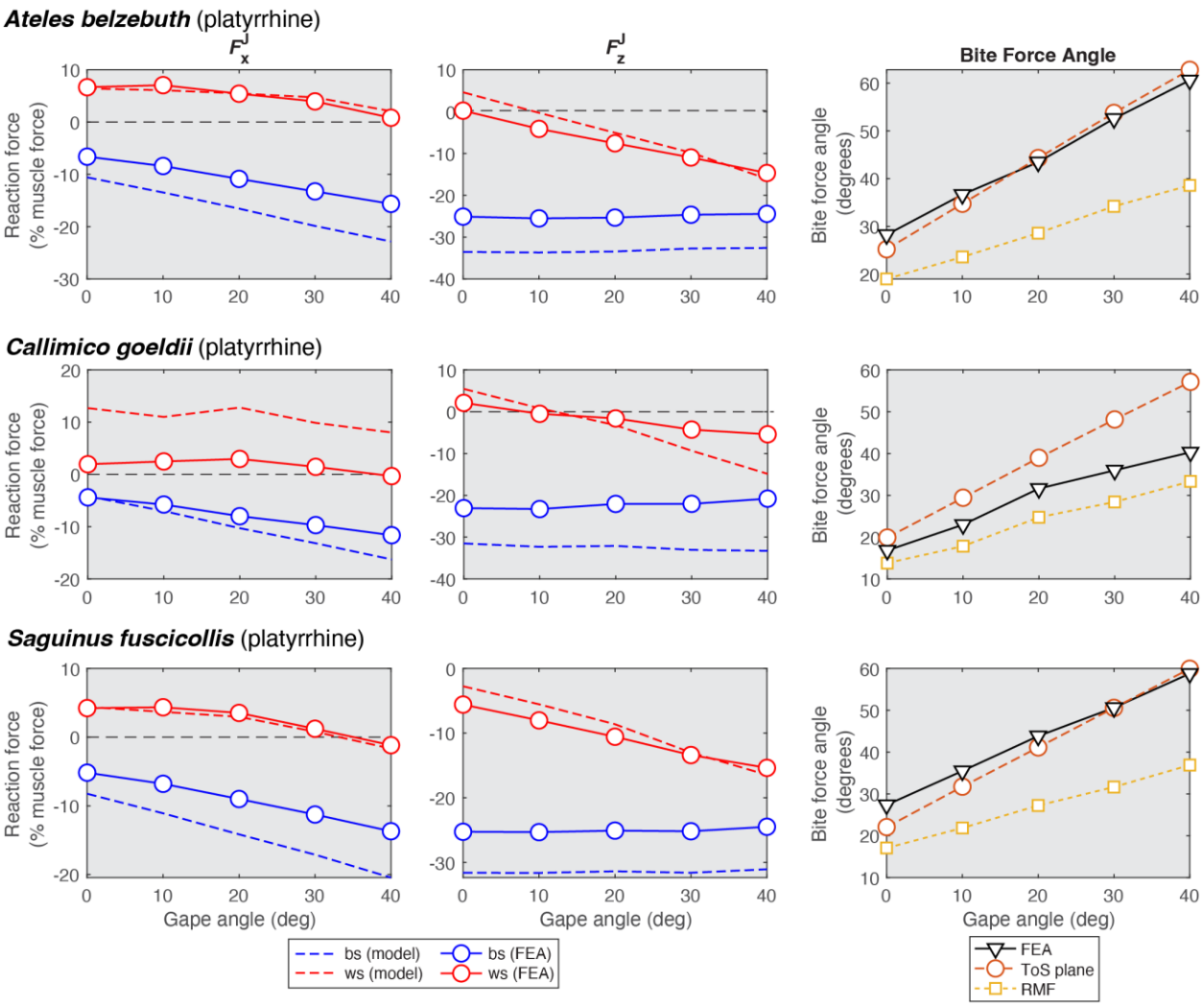

Fig. S3. Comparison between the mathematical and the FEA models. (continuation)

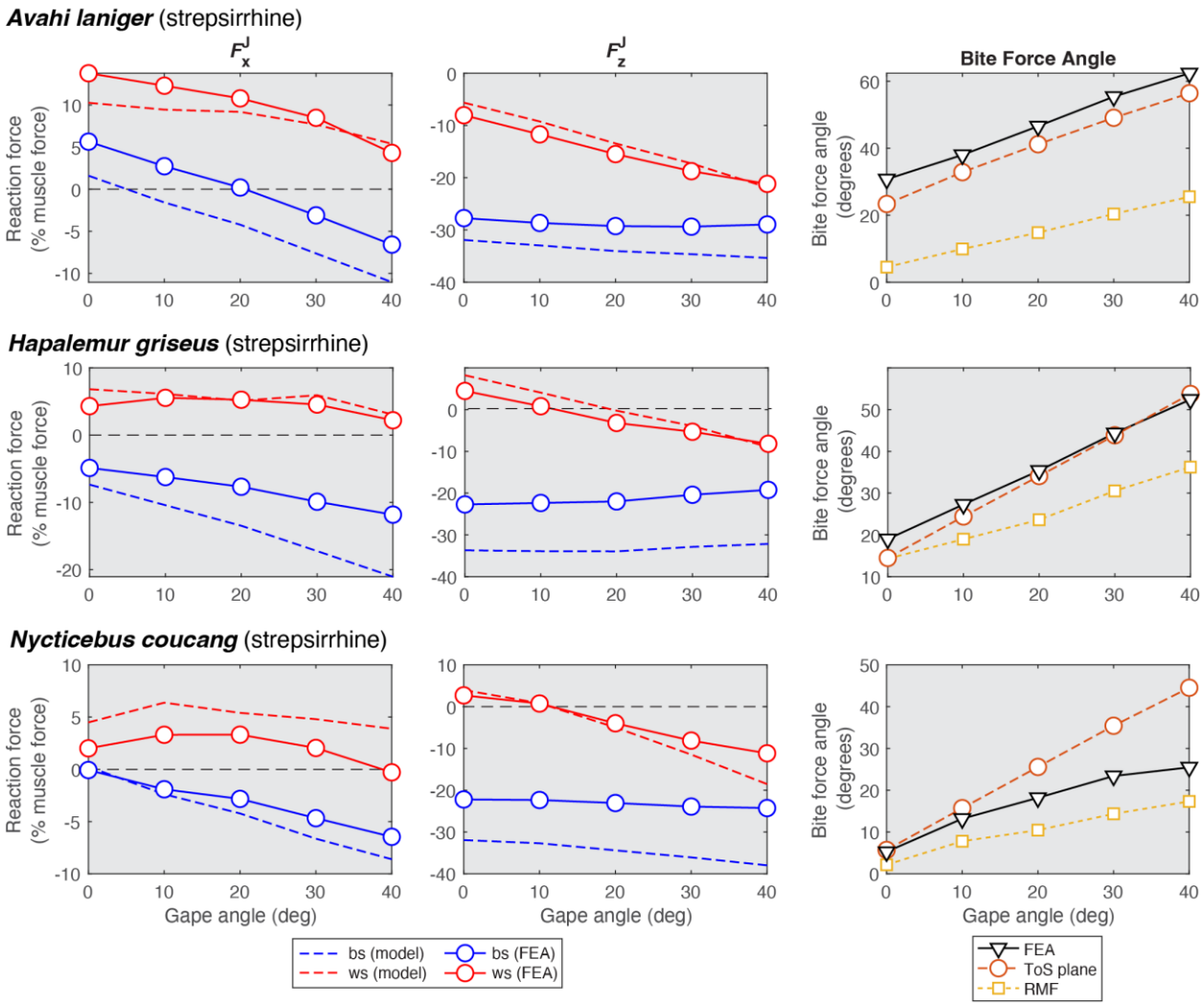

Fig. S3. Comparison between the mathematical and the FEA models. (continuation)

References

Gingerich, P. D. (1979). The human mandible: Lever, link, or both? *Am. J. Phys. Anthropol.* **51**, 135–137.

Hylander, W. L. (1975). The human mandible: Lever or link? *Am. J. Phys. Anthropol.* **43**, 227–242.

Maas, S. A., Ellis, B. J., Ateshian, G. A. and Weiss, J. A. (2012). FEBio: Finite elements for biomechanics. *J. Biomech. Eng.* **134**, 011005.

Moerman, K. M. (2018). GIBBON: The geometry and image-based bioengineering add-on. *J. Open Source Softw.* **3**, 506.

Si, H. (2015). TetGen, a Delaunay-based quality tetrahedral mesh generator. *ACM Trans. Math. Softw.* **41**, 1–36.

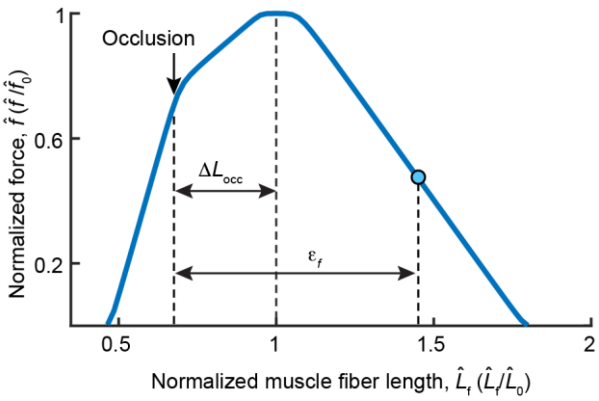

Fig. S4. Length–tension curve. The curve shows the relationship between the normalized muscle fiber length ($\hat{L}_f$) and the ability of the muscle fiber to generate relative active force ($\hat{f}$). The blue circle indicates the relative amount of force that a muscle fiber would generate if it were stretched an amount ε_f from its length at occlusion. $\hat{L}_0$ represents the optimal fiber length where maximal tetanic force ($\hat{f}_0$) is generated. The occlusal offset length, ΔL_{occ}, is the difference in fiber length between occlusion and its optimal length.

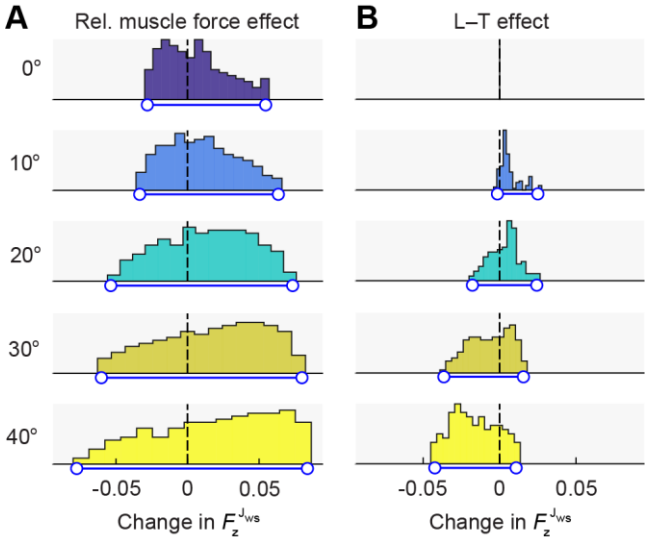

Fig. S5. Effect of variation in different model inputs on the working-side vertical joint reaction force (F_z^{Jws}) at different gapes for *Pan paniscus*. (A) The distribution of the effect of varying the relative muscle force configuration with respect to the reference configuration (i.e., all muscles generate the same relative force). **(B)** Distribution of the effect of gape-dependent changes in muscle force generation with respect to the condition where muscle force is constant regardless of gape. Because the L–T effect is calculated based on the differential stretch of muscle segments with gapes, there is no variation at 0° gape (i.e., at occlusion). The blue lines at the bottom of each distribution represent the range of the effect, a measure of the relative importance of the effect.

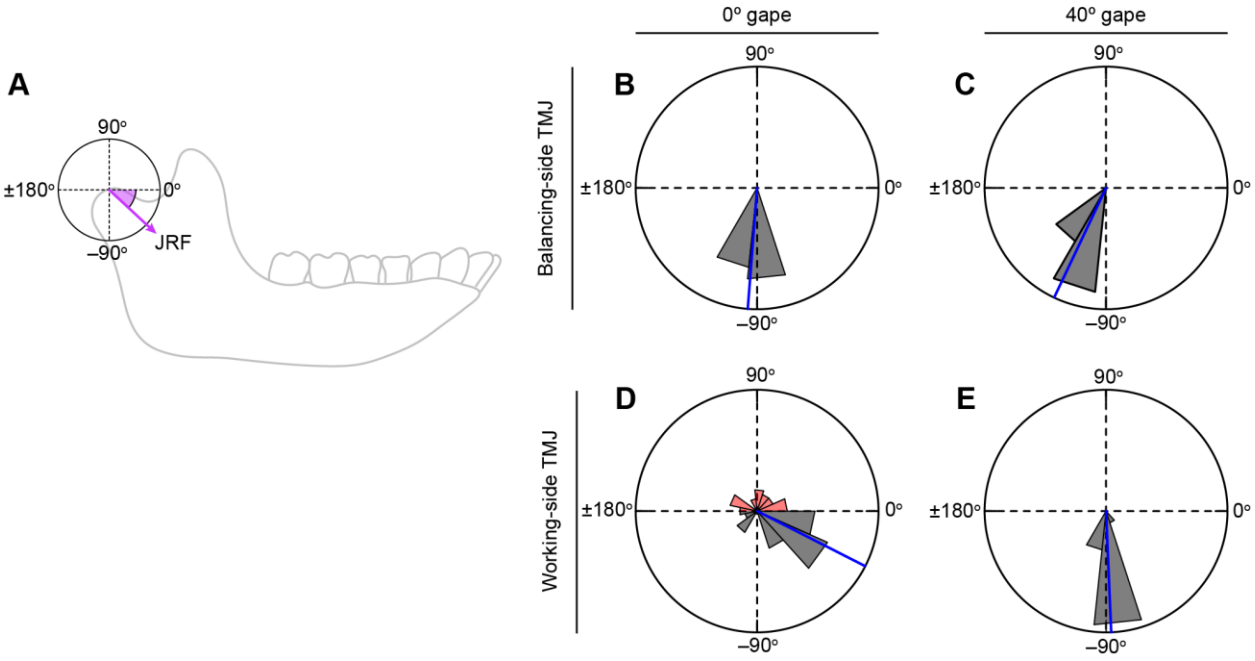

Fig. S6. Joint reaction force angle. (A) Lateral view of the mandible depicting angle of the JRF (purple arrow). Note that a JRF pointing downward, as shown here, represents the reacting force of the condyle pushing upwards and backwards on the cranium. Thus, a negative JRF angle represents a compressive JRF, while a positive angle indicates a distracting force. **(B–E)** Rose diagrams of the distribution of JRF angles of all 97 primate species for the balancing- and working-side TMJs at 0° and 40° gapes. The length of each bin represents the relative frequency of species within each angular bin. Bins in red indicate species that experience distracting forces. The solid blue line represents the mean angular value.

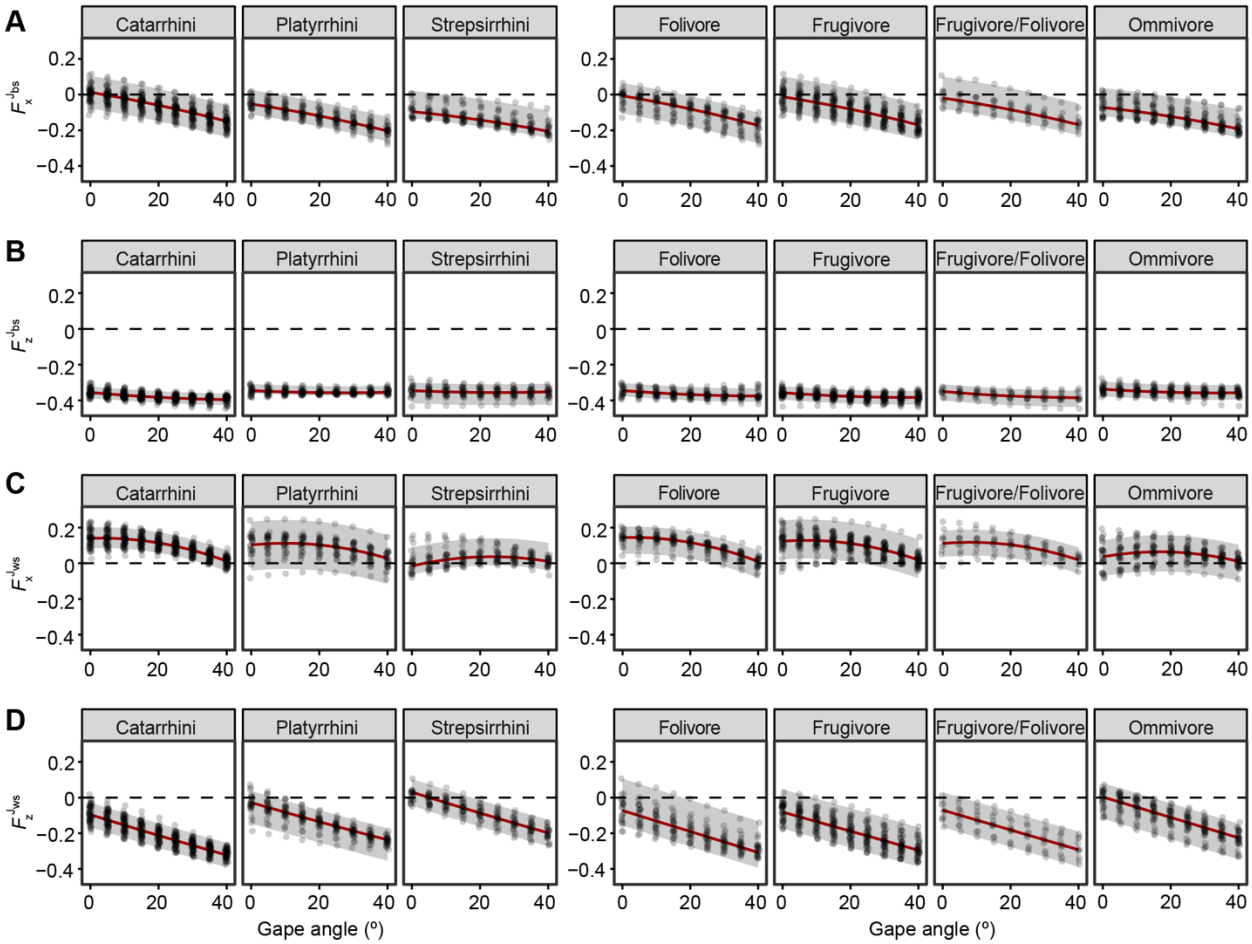

Fig. S7. Relationship between gape angle and the joint reaction forces by taxonomic and dietary category. Relationship between gape angle and the **(A)** balancing–side horizontal JRF, **(B)** the balancing–side vertical JRF, **(C)** the working–side horizontal JRF, and **(D)** the working–side vertical JRF. The red line represents the Bayesian regression fit, and the shaded areas are the 95% credible intervals.

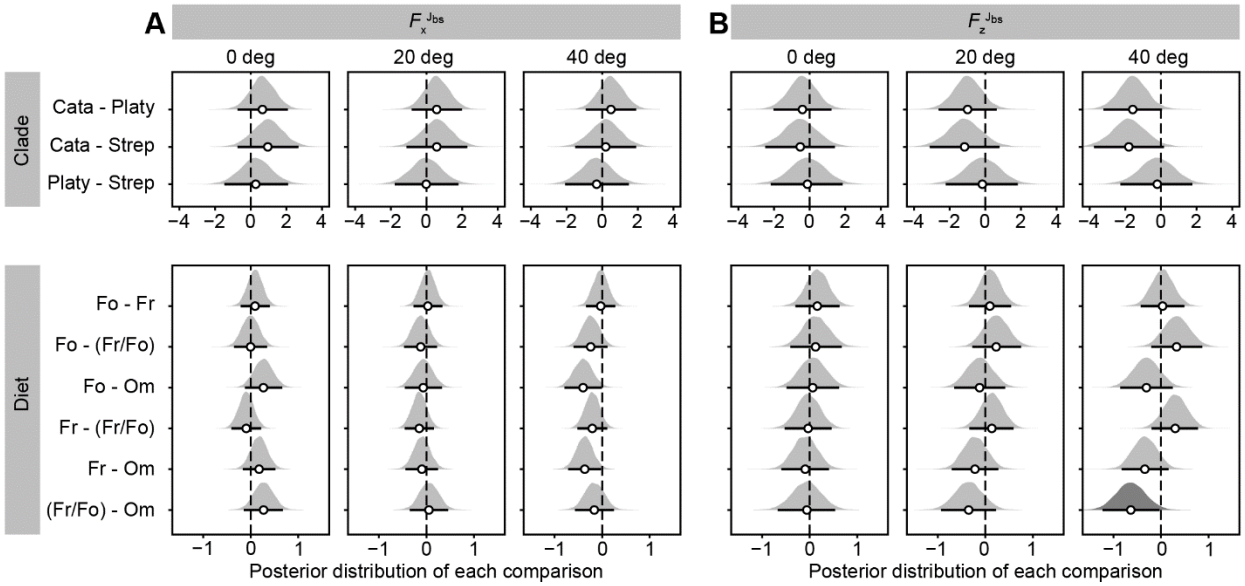

Fig. S8. Posterior distributions of comparisons at different gape angles between taxonomic and dietary categories for the horizontal (A) and vertical (B) balancing–side JRFs. Circles and horizontal solid black lines represent the median and the 95% HDI of the posterior distribution, respectively. Distributions that are shaded in dark gray indicate that the comparison is significant (pd>97.5% and % in ROPE < 2.5). Abbreviations: Cata=catarrhines, Platy=platyrrhines, Strep=strepsirrhines, Fo=folivores, Fr=frugivores, Fr/Fo=frugivore/folivores, Om=omnivores.

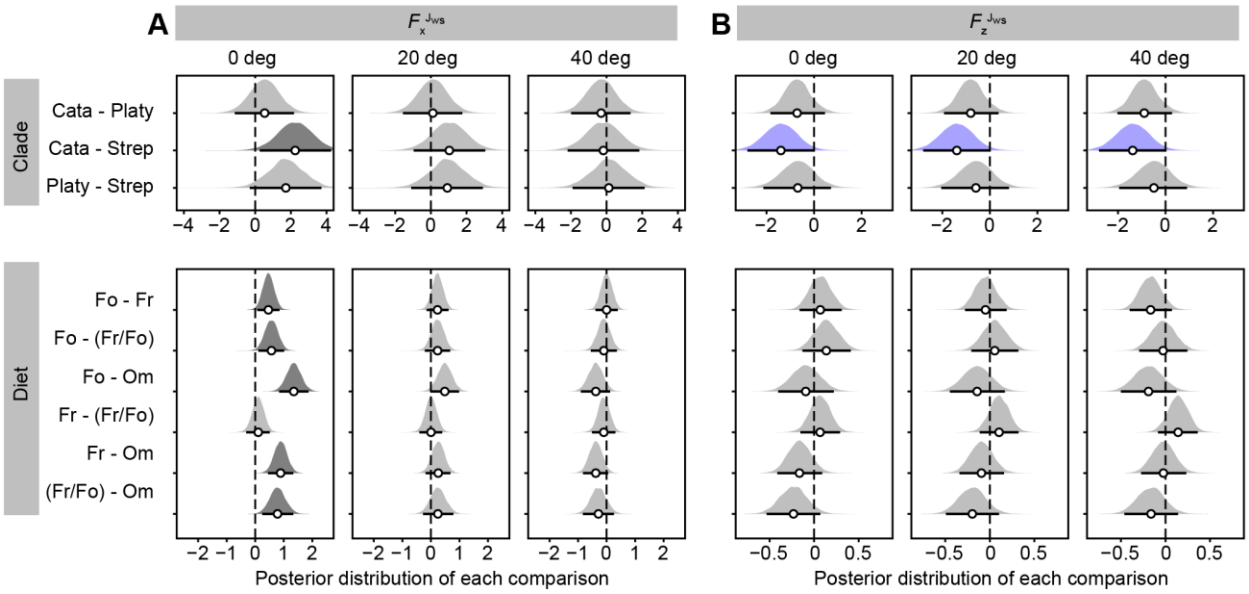

Fig. S9. Posterior distributions of comparisons at different gape angles between taxonomic and dietary categories for the horizontal (A) and vertical (B) working–side JRFs. Circles and horizontal solid black lines represent the median and the 95% HDI of the posterior distribution, respectively. Distributions that are shaded in either dark gray or blue indicate that the comparison is significant (pd>97.5% and % in ROPE < 2.5). Distributions that are shaded blue indicate that the comparison is significant for all three gape angles. Abbreviations as in **Fig. S8**.

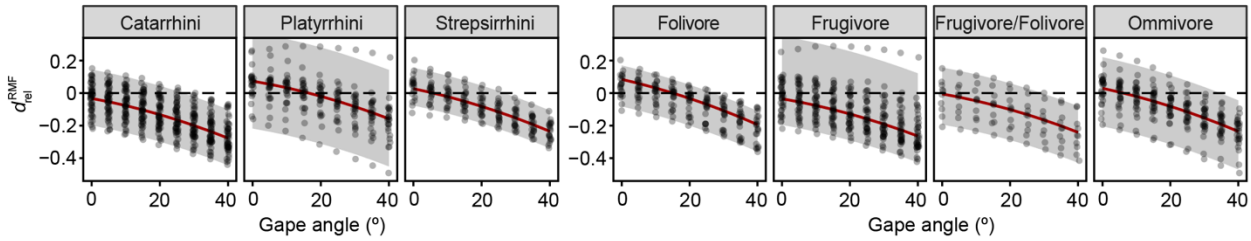

Fig. S10. Relationship between gape angle and the position of the RMF by taxonomic and dietary category. The red line represents the Bayesian regression fit, and the shaded areas are the 95% credible intervals.

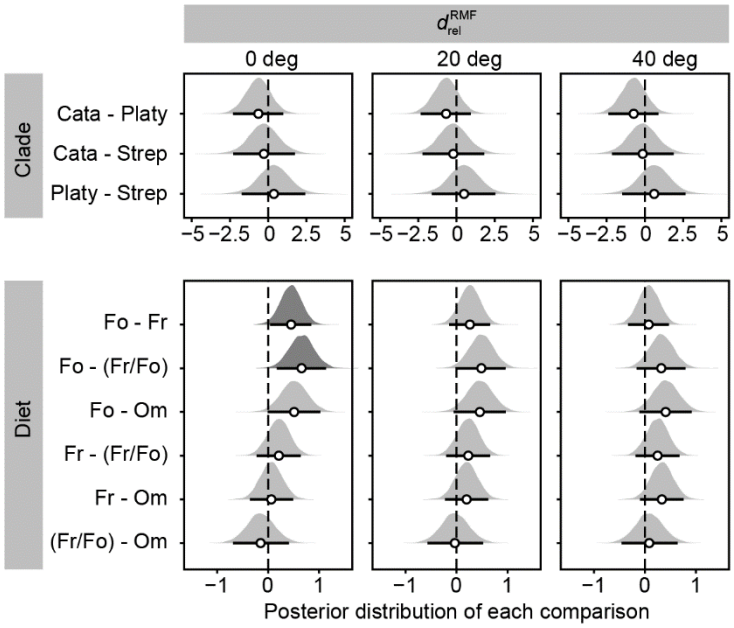

Fig. S11. Posterior distributions of comparisons at different gape angles between taxonomic and dietary categories for the resultant muscle force (RMF). Circles and horizontal solid black lines represent the median and the 95% HDI of the posterior distribution, respectively. Distributions that are shaded in dark gray indicate that the comparison is significant (pd>97.5% and % in ROPE < 2.5). Abbreviations as in **Fig. S8**.

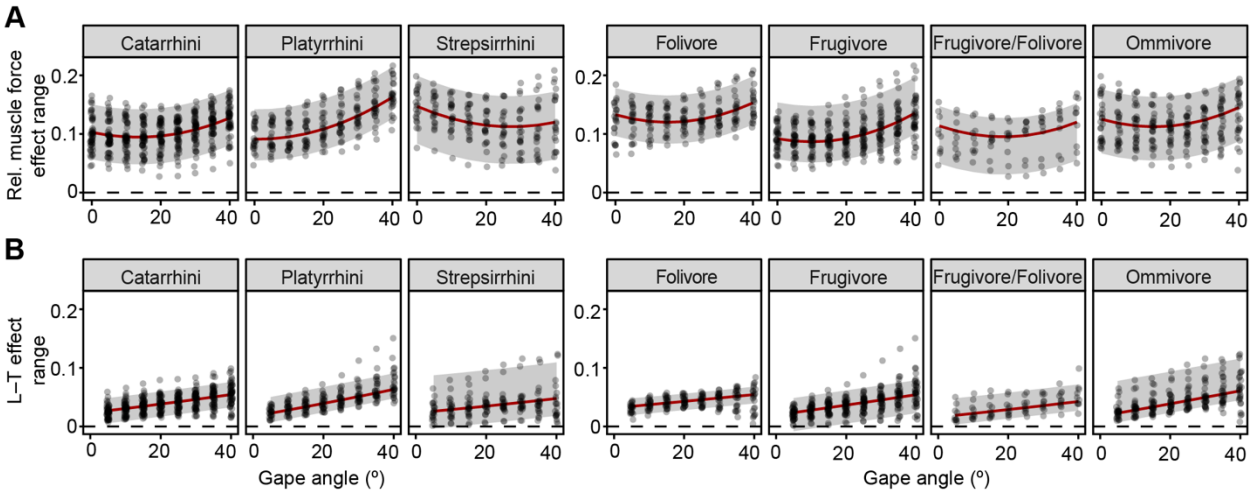

Fig. S12. Relationship between gape angle and the range of the PCSA effect (A) and the range of the L–T effect (B). The red line represents the Bayesian regression fit, and the shaded areas are the 95% credible intervals.

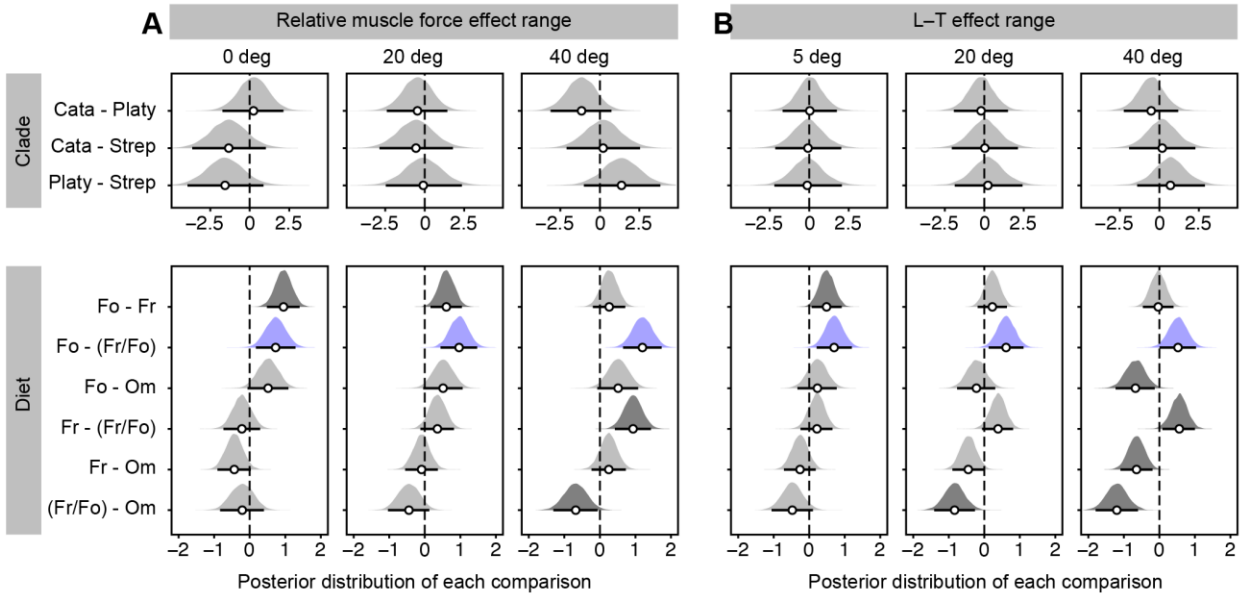

Fig. S13. Posterior distributions of comparisons at different gape angles between taxonomic and dietary categories for the ranges of the relative muscle force effect (A) and the L–T effect (B). Circles and horizontal solid black lines represent the median and the 95% HDI of the posterior distribution, respectively. Distributions that are shaded in either dark gray or blue indicate that the comparison is significant (pd>97.5% and % in ROPE < 2.5). Distributions that are shaded blue indicate that the comparison is significant for all three gape angles. Abbreviations as in **Fig. S8**.

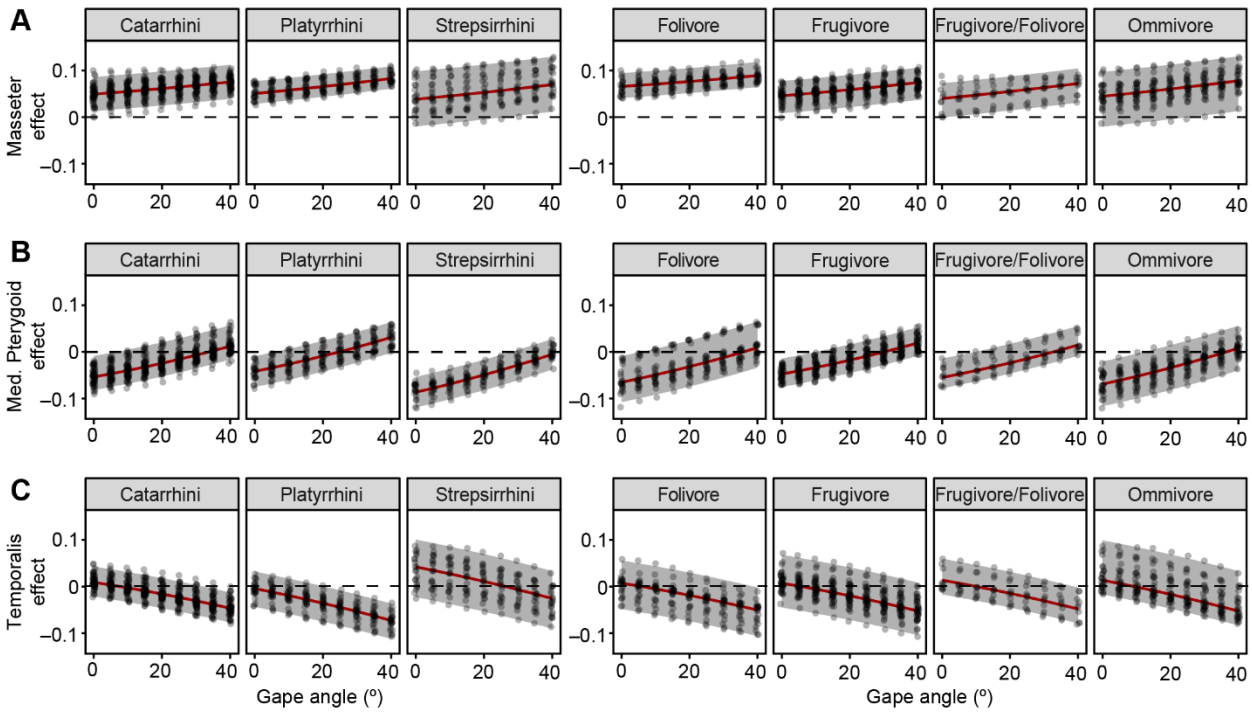

Fig. S14. Effect of gape on the muscle effect on the working–side vertical JRF by clade and dietary category. Relationship between gape angle and **(A)** the effect of masseter muscle on F_z^{Jws}, **(B)** the effect of the medial pterygoid muscle on F_z^{Jws}, and **(C)** the effect of the temporalis muscle on F_z^{Jws}. The red line represents the Bayesian regression fit, and the shaded areas are the 95% credible intervals.

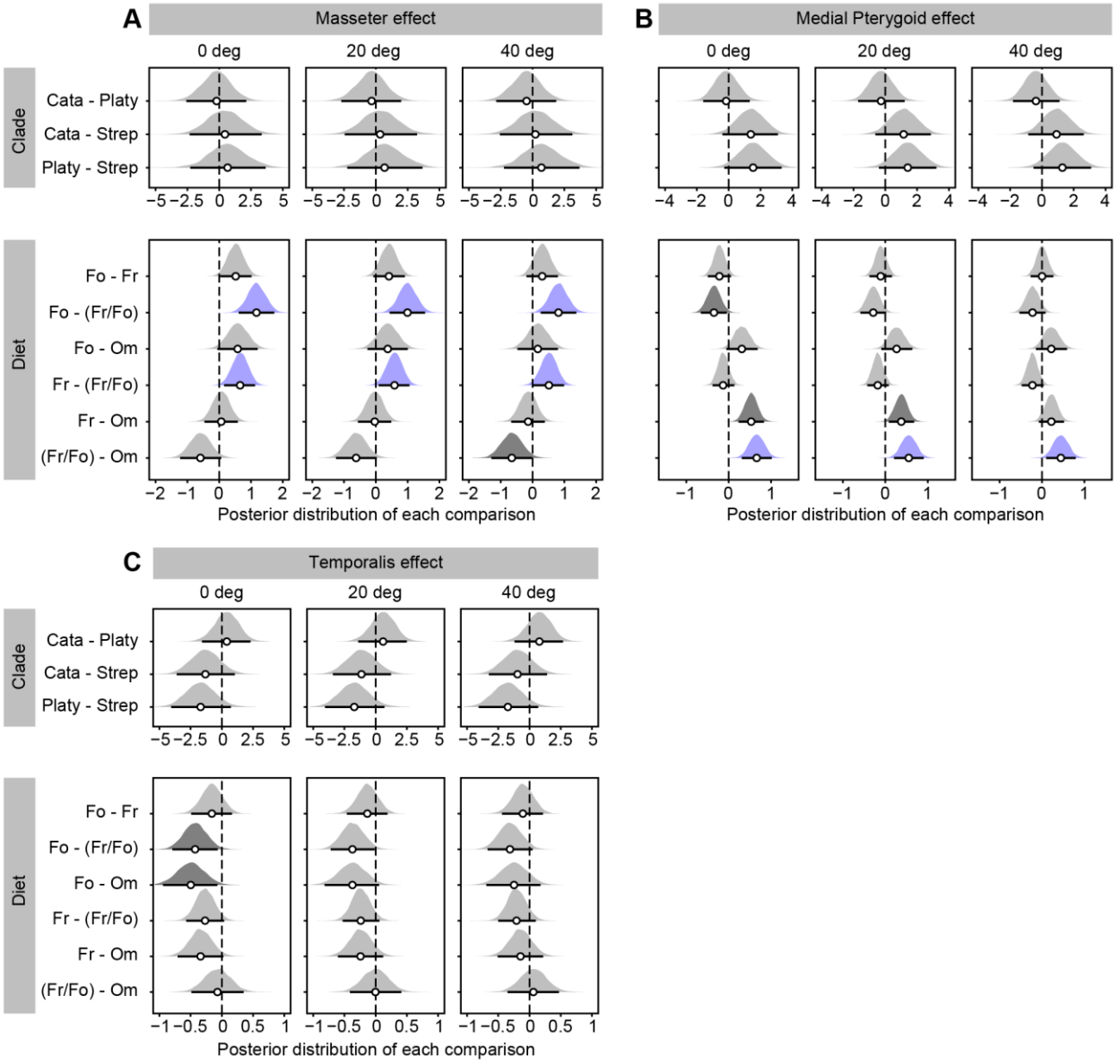

Fig. S15. Posterior distributions of comparisons at different gape angles between taxonomic and dietary categories for the muscle effects of the masseter (A), medial pterygoid (B), and the temporalis (C). Circles and horizontal solid black lines represent the median and the 95% HDI of the posterior distribution, respectively. Distributions that are shaded in either dark gray or blue indicate that the comparison is significant (pd>97.5% and % in ROPE < 2.5). Distributions that are shaded blue indicate that the comparison is significant for all three gape angles. Abbreviations as in **Fig. S8**.

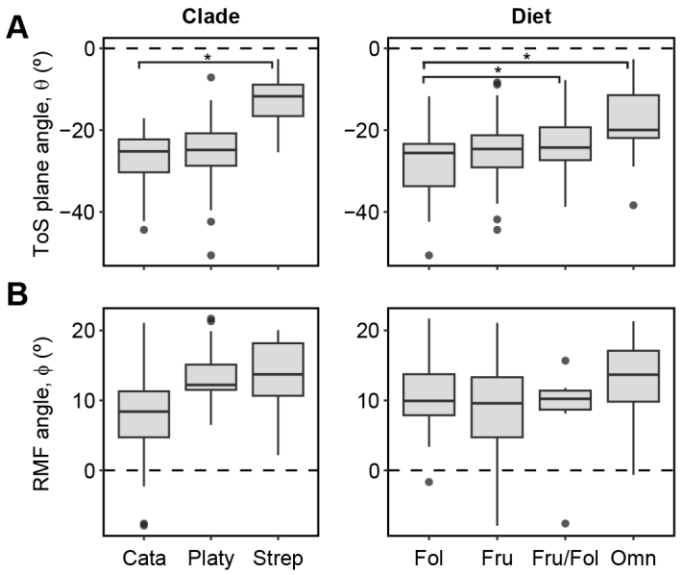

Fig. S16. Boxplots of the effect of clade and diet on the ToS plane angle (A) and the RMF angle (B). Cata = catarrhines, Platy = platyrrhines, Strep = strepsirrhines, Fol = folivores, Fru = frugivores, Fru/Fol = Frugivores/folivores, and Omn = omnivores. Asterisks indicate statistically significant differences (pd > 97.5% and % in ROPE < 2.5).

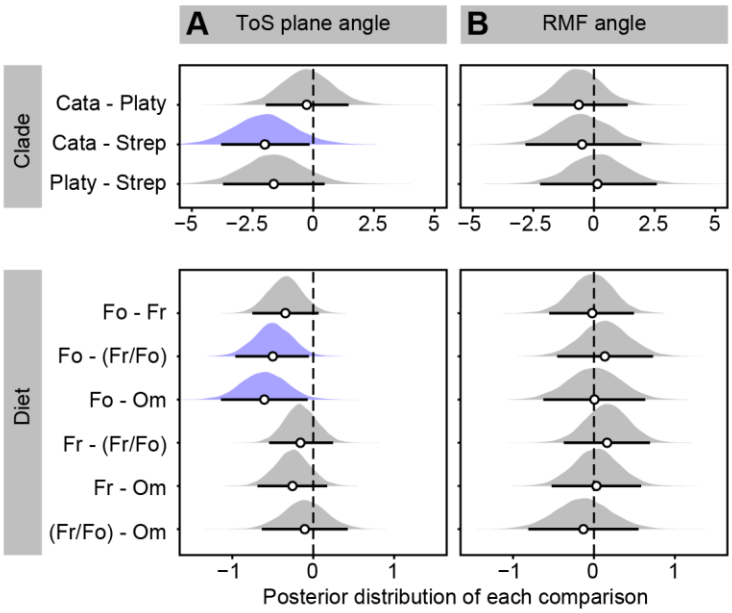

Fig. S17. Posterior distributions of the comparisons between taxonomic and dietary categories for the ToS plane angle (A) and the RMF angle (B). Circles and horizontal solid black lines represent the median and the 95% HDI of the posterior distribution, respectively. Distributions that are shaded in either dark gray or blue indicate that the comparison is significant (pd>97.5% and % in ROPE < 2.5). Distributions that are shaded blue indicate that the comparison is significant for all three gape angles. Abbreviations as in **Fig. S8**.

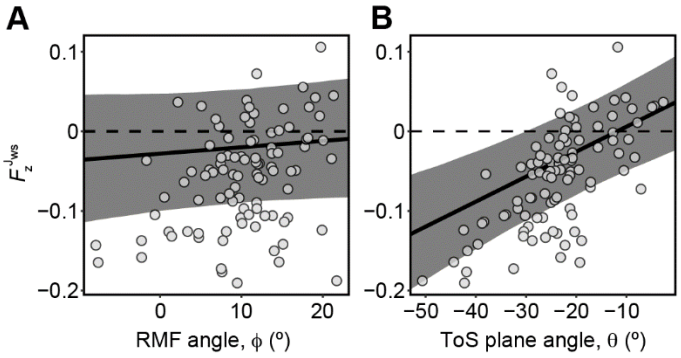

Fig. S18. Relationships between the working–side vertical joint reaction force and the RMF angle (A) and the ToS plane angle (B). The black lines represent the Bayesian regression fits, and the shaded areas correspond to their 95% credible intervals.

Table S1. Summary statistics of Bayesian regressions of the balancing-side joint reaction forces modeled as a function of *gape angle* and (*gape angle*)^2 as covariates.

	F_x^{Jbs}		F_z^{Jbs}	
Marginal R^2	0.49		0.11	
Conditional R^2	0.98		0.83	
Phylogenetic λ	0.85		0.72	
	Median	**95% HDI**	**Median**	**95% HDI**
Intercept	–0.14	[–0.91, 0.60]	0.31	[–0.57, 1.22]
(Gape angle)^2	–0.06	[–0.07, –0.05]	0.12	[0.08, 0.15]
Gape angle	–0.71	[–0.72, –0.69]	–0.31	[–0.34, –0.29]

Estimates for the intercepts represent the estimated marginal means calculated by the 'emmeans' function (*emmeans* package). 95% HDI represents the 95% highest density interval. Coefficients of covariates with strong support (i.e., 95% HDI that does not contain zero) are highlighted. All variables were standardized.

Table S2. Summary statistics of Bayesian regressions of the working-side joint reaction forces modeled as a function of *gape angle* and (*gape angle*)^2 as covariates.

	F_x^{Jws}		F_z^{Jws}	
Marginal R^2	0.29		0.56	
Conditional R^2	0.85		0.98	
Phylogenetic λ	0.8		0.91	
	Median	**95% HDI**	**Median**	**95% HDI**
Intercept	–0.09	[–0.98, 0.79]	0.45	[–0.19, 1.10]
(Gape angle)^2	–0.26	[–0.29, –0.23]	0.02	[0.01, 0.03]
Gape angle	–0.50	[–0.52, –0.48]	–0.76	[–0.77, –0.75]

Estimates for the intercepts represent the estimated marginal means calculated by the 'emmeans' function (*emmeans* package). 95% HDI represents the 95% highest density interval. Coefficients of covariates with strong support (i.e., 95% HDI that does not contain zero) are highlighted. All variables were standardized.

Table S3. Summary statistics of Bayesian regressions of the relative position of the resultant muscle force modeled as a function of *gape angle* and (*gape angle*)^2 as covariates.

	$d_{\mathrm{rel}}^{\mathrm{RMF}}$	
Marginal R^2	0.39	
Conditional R^2	0.97	
Phylogenetic λ	0.76	
	Median	**95% HDI**
Intercept	0.21	[–0.68, 1.11]
(Gape angle)^2	–0.07	[–0.08, –0.06]
Gape angle	–0.62	[–0.63, –0.61]

Estimates for the intercepts represent the estimated marginal means calculated by the 'emmeans' function (*emmeans* package). 95% HDI represents the 95% highest density interval. Coefficients of covariates with strong support (i.e., 95% HDI that does not contain zero) are highlighted. All variables were standardized.

Table S4. Summary statistics of Bayesian regressions of the effect ranges modeled as a function of *gape angle* and (*gape angle*)^2 as covariates.

	Rel. muscle force effect range		**L–T effect range**	
Marginal R^2	0.13		0.23	
Conditional R^2	0.71		0.76	
Phylogenetic λ	0.75		0.65	
	Median	**95% HDI**	**Median**	**95% HDI**
Intercept	0.12	[–0.91, 1.18]	0.04	[–0.80, 0.88]
(Gape angle)^2	0.26	[0.22, 0.30]	0.00	[–0.02, 0.03]
Gape angle	0.29	[0.25, 0.32]	0.47	[0.45, 0.50]

Estimates for the intercepts represent the estimated marginal means calculated by the 'emmeans' function (*emmeans* package). 95% HDI represents the 95% highest density interval. Coefficients of covariates with strong support (i.e., 95% HDI that does not contain zero) are highlighted. All variables were standardized.

Table S5. Summary statistics of Bayesian regressions of the muscle effects modeled as a function of *gape angle* and (*gape angle*)^2 as covariates.

	Masseter effect		**Med. pterygoid effect**		**Temporalis effect**	
Marginal R^2	0.16		0.51		0.36	
Conditional R^2	0.98		0.98		0.98	
Phylogenetic λ	0.84		0.92		0.95	
	Median	**95% HDI**	**Median**	**95% HDI**	**Median**	**95% HDI**
Intercept	–0.15	[–1.42, 1.08]	–0.46	[–1.26, 0.34]	0.45	[–0.61, 1.51]
(Gape angle)^2	0.02	[0.01, 0.03]	0.05	[0.04, 0.06]	–0.03	[–0.04, –0.02]
Gape angle	0.40	[0.39, 0.41]	0.70	[0.69, 0.71]	–0.59	[–0.60, –0.58]

Estimates for the intercepts represent the estimated marginal means calculated by the 'emmeans' function (*emmeans* package). 95% HDI represents the 95% highest density interval. Coefficients of covariates with strong support (i.e., 95% HDI that does not contain zero) are highlighted. All variables were standardized.

Table S6. Summary statistics of Bayesian regressions of the balancing-side joint reaction forces modeled as a function of *gape angle* and (*gape angle*)^2 as covariates, and *clade* as a fixed effect.

	F_x^{Jbs}		F_z^{Jbs}	
Marginal R^2	0.60		0.42	
Conditional R^2	0.98		0.87	
Phylogenetic λ	0.87		0.71	
	Median	**95% HDI**	**Median**	**95% HDI**
Covariate				
(Gape angle)^2	–0.05	[–0.06, –0.04]	0.11	[0.08, 0.14]
Gape angle				
Catarrhini	–0.76	[–0.77, –0.75]	–0.50	[–0.53, –0.46]
Platyrrhini	–0.71	[–0.74, –0.67]	–0.11	[–0.21, –0.02]
Strepsirrhini	–0.52	[–0.55, –0.48]	–0.09	[–0.18, 0.01]
Intercept				
Catarrhini	0.29	[–1.08, 1.67]	–0.56	[–2.13, 1.02]
Platyrrhini	–0.28	[–3.08, 2.50]	0.43	[–2.77, 3.65]
Strepsirrhini	–0.28	[–3.37, 2.79]	0.61	[–2.92, 4.14]

Estimates for the intercepts represent the estimated marginal means calculated by the 'emmeans' function (*emmeans* package). 95% HDI represents the 95% highest density interval. Coefficients of covariates with strong support (i.e., 95% HDI that does not contain zero) are highlighted. All variables were standardized.

Table S7. Summary statistics of Bayesian regressions of the working-side joint reaction forces modeled as a function of *gape angle* and (*gape angle*)^2 as covariates, and *clade* as a fixed effect.

	F_x^{Jws}		F_z^{Jws}	
Marginal R^2	0.50		0.79	
Conditional R^2	0.92		0.98	
Phylogenetic λ	0.83		0.90	
	Median	**95% HDI**	**Median**	**95% HDI**
Covariate				
(Gape angle)^2	–0.25	[–0.27, –0.23]	0.02	[0.01, 0.02]
Gape angle				
Catarrhini	–0.66	[–0.68, –0.63]	–0.77	[–0.78, –0.76]
Platyrrhini	–0.39	[–0.45, –0.33]	–0.71	[–0.75, –0.68]
Strepsirrhini	0.13	[0.06, 0.19]	–0.78	[–0.81, –0.74]
Intercept				
Catarrhini	0.54	[–1.09, 2.14]	–0.53	[–1.64, 0.61]
Platyrrhini	0.43	[–2.85, 3.71]	0.28	[–2.00, 2.53]
Strepsirrhini	–0.49	[–4.13, 3.11]	0.86	[–1.62, 3.41]

Estimates for the intercepts represent the estimated marginal means calculated by the 'emmeans' function (*emmeans* package). 95% HDI represents the 95% highest density interval. Coefficients of covariates with strong support (i.e., 95% HDI that does not contain zero) are highlighted. All variables were standardized.

Table S8. Summary statistics of Bayesian regressions of the balancing-side joint reaction forces modeled as a function of *gape angle* and (*gape angle*)^2 as covariates, and *diet* as a fixed effect.

	F_x^{Jbs}		F_z^{Jbs}	
Marginal R^2	0.49		0.15	
Conditional R^2	0.99		0.82	
Phylogenetic λ	0.73		0.68	
	Median	**95% HDI**	**Median**	**95% HDI**
Covariate				
(Gape angle)^2	–0.06	[–0.07, –0.04]	0.12	[0.09, 0.15]
Gape angle				
Folivore	–0.78	[–0.79, –0.76]	–0.37	[–0.44, –0.30]
Frugivore	–0.74	[–0.78, –0.69]	–0.33	[–0.48, –0.17]
Frugivore/Folivore	–0.70	[–0.76, –0.65]	–0.43	[–0.61, –0.25]
Omnivore	–0.56	[–0.61, –0.51]	–0.25	[–0.40, –0.09]
Intercept				
Folivore	–0.19	[–0.99, 0.62]	0.29	[–0.64, 1.25]
Frugivore	–0.22	[–1.33, 0.89]	0.20	[–1.18, 1.60]
Frugivore/Folivore	–0.07	[–1.21, 1.09]	0.06	[–1.39, 1.53]
Omnivore	–0.12	[–1.32, 1.07]	0.41	[–1.05, 1.91]

Estimates for the intercepts represent the estimated marginal means calculated by the 'emmeans' function (*emmeans* package). 95% HDI represents the 95% highest density interval. Coefficients of covariates with strong support (i.e., 95% HDI that does not contain zero) are highlighted. All variables were standardized.

Table S9. Summary statistics of Bayesian regressions of the working-side joint reaction forces modeled as a function of *gape angle* and (*gape angle*)^2 as covariates, and *diet* as a fixed effect.

	F_x^{Jws}		F_z^{Jws}	
Marginal R^2	0.35		0.59	
Conditional R^2	0.89		0.98	
Phylogenetic λ	0.76		0.9	
	Median	**95% HDI**	**Median**	**95% HDI**
Covariate				
(Gape angle)^2	–0.26	[–0.29, –0.24]	0.02	[0.01, 0.02]
Gape angle				
Folivore	–0.69	[–0.73, –0.65]	–0.80	[–0.83, –0.78]
Frugivore	–0.54	[–0.63, –0.46]	–0.73	[–0.78, –0.68]
Frugivore/Folivore	–0.48	[–0.58, –0.37]	–0.76	[–0.81, –0.70]
Omnivore	–0.13	[–0.23, –0.03]	–0.78	[–0.82, –0.73]
Intercept				
Folivore	0.24	[–0.69, 1.13]	0.38	[–0.29, 1.05]
Frugivore	0.01	[–1.31, 1.28]	0.42	[–0.48, 1.34]
Frugivore/Folivore	0.00	[–1.36, 1.34]	0.32	[–0.61, 1.26]
Omnivore	–0.25	[–1.68, 1.15]	0.52	[–0.45, 1.50]

Estimates for the intercepts represent the estimated marginal means calculated by the 'emmeans' function (*emmeans* package). 95% HDI represents the 95% highest density interval. Coefficients of covariates with strong support (i.e., 95% HDI that does not contain zero) are highlighted. All variables were standardized.

Table S10. Summary statistics of Bayesian regressions of the position of the resultant muscle force vector modeled as a function of *gape angle* and (*gape angle*)^2 as covariates, and *clade* as a fixed effect.

	$d_{\mathrm{rel}}^{\mathrm{RMF}}$	
Marginal R^2	0.48	
Conditional R^2	0.97	
Phylogenetic λ	0.78	
	Median	**95% HDI**
Covariate		
(Gape angle)^2	–0.07	[–0.08, –0.06]
Gape angle		
Catarrhini	–0.61	[–0.63, –0.60]
Platyrrhini	–0.58	[–0.63, –0.54]
Strepsirrhini	–0.66	[–0.70, –0.62]
Intercept		
Catarrhini	–0.04	[–1.62, 1.58]
Platyrrhini	0.65	[–2.54, 3.92]
Strepsirrhini	0.17	[–3.43, 3.80]

Estimates for the intercepts represent the estimated marginal means calculated by the 'emmeans' function (*emmeans* package). 95% HDI represents the 95% highest density interval. Coefficients of covariates with strong support (i.e., 95% HDI that does not contain zero) are highlighted. All variables were standardized.

Table S11. Summary statistics of Bayesian regressions of the position of the resultant muscle force vector modeled as a function of *gape angle* and (*gape angle*)^2 as covariates, and *diet* as a fixed effect.

	$d_{\mathrm{rel}}^{\mathrm{RMF}}$	
Marginal R^2	0.42	
Conditional R^2	0.97	
Phylogenetic λ	0.76	
	Median	**95% HDI**
Covariate		
(Gape angle)^2	–0.07	[–0.08, –0.06]
Gape angle		
Folivore	–0.70	[–0.72, –0.67]
Frugivore	–0.58	[–0.63, –0.52]
Frugivore/Folivore	–0.59	[–0.65, –0.53]
Omnivore	–0.66	[–0.72, –0.61]
Intercept		
Folivore	0.54	[–0.43, 1.49]
Frugivore	0.28	[–1.09, 1.63]
Frugivore/Folivore	0.05	[–1.39, 1.48]
Omnivore	0.08	[–1.40, 1.54]

Estimates for the intercepts represent the estimated marginal means calculated by the 'emmeans' function (*emmeans* package). 95% HDI represents the 95% highest density interval. Coefficients of covariates with strong support (i.e., 95% HDI that does not contain zero) are highlighted. All variables were standardized.

Table S12. Summary statistics of Bayesian regressions of the effect ranges modeled as a function of *gape angle* and (*gape angle*)^2 as covariates, and *clade* as a fixed effect.

	Rel. muscle force effect range		**L–T effect range**	
Marginal R^2	0.34		0.32	
Conditional R^2	0.82		0.79	
Phylogenetic λ	0.78		0.75	
	Median	**95% HDI**	**Median**	**95% HDI**
Covariate				
(Gape angle)^2	0.23	[0.20, 0.26]	0.01	[–0.01, 0.04]
Gape angle				
Catarrhini	0.23	[0.20, 0.27]	0.44	[0.41, 0.47]
Platyrrhini	0.69	[0.59, 0.78]	0.65	[0.57, 0.73]
Strepsirrhini	–0.26	[–0.40, –0.12]	0.35	[0.25, 0.44]
Intercept				
Catarrhini	–0.37	[–2.23, 1.50]	0.00	[–1.67, 1.69]
Platyrrhini	0.09	[–3.66, 3.90]	0.20	[–3.17, 3.61]
Strepsirrhini	0.19	[–4.01, 4.37]	–0.04	[–3.80, 3.74]

Estimates for the intercepts represent the estimated marginal means calculated by the 'emmeans' function (*emmeans* package). 95% HDI represents the 95% highest density interval. Coefficients of covariates with strong support (i.e., 95% HDI that does not contain zero) are highlighted. All variables were standardized.

Table S13. Summary statistics of Bayesian regressions of the effect ranges modeled as a function of *gape angle* and (*gape angle*)^2 as covariates, and *diet* as a fixed effect.

	Rel. muscle force effect range		L–T effect range	
Marginal R^2	0.23		0.30	
Conditional R^2	0.72		0.78	
Phylogenetic λ	0.75		0.77	
	Median	**95% HDI**	**Median**	**95% HDI**
Covariate				
(Gape angle)^2	0.27	[0.24, 0.31]	0.00	[–0.02, 0.03]
Gape angle				
Folivore	0.20	[0.13, 0.27]	0.32	[0.26, 0.37]
Frugivore	0.42	[0.26, 0.57]	0.49	[0.37, 0.60]
Frugivore/Folivore	0.04	[–0.16, 0.26]	0.38	[0.24, 0.51]
Omnivore	0.20	[0.03, 0.36]	0.61	[0.49, 0.73]
Intercept				
Folivore	0.59	[–0.46, 1.63]	0.04	[–0.99, 1.02]
Frugivore	–0.02	[–1.50, 1.47]	–0.19	[–1.63, 1.21]
Frugivore/Folivore	–0.38	[–1.93, 1.19]	–0.57	[–2.09, 0.90]
Omnivore	0.07	[–1.52, 1.68]	0.26	[–1.30, 1.79]

Estimates for the intercepts represent the estimated marginal means calculated by the 'emmeans' function (*emmeans* package). 95% HDI represents the 95% highest density interval. Coefficients of covariates with strong support (i.e., 95% HDI that does not contain zero) are highlighted. All variables were standardized.

Table S14. Summary statistics of Bayesian regressions of the muscle effects modeled as a function of *gape angle* and (*gape angle*)^2 as covariates, and *clade* as a fixed effect.

	Masseter effect		Med. pterygoid effect		Temporalis effect	
Marginal R^2	0.32		0.66		0.58	
Conditional R^2	0.98		0.98		0.99	
Phylogenetic λ	0.86		0.92		0.96	
	Median	**95% HDI**	**Median**	**95% HDI**	**Median**	**95% HDI**
Covariate						
(Gape angle)^2	0.02	[0.01, 0.03]	0.05	[0.04, 0.06]	–0.04	[–0.04, 0.03]
Gape angle						
Catarrhini	0.36	[0.35, 0.38]	0.65	[0.64, 0.66]	–0.54	[–0.55, 0.53]
Platyrrhini	0.45	[0.41, 0.48]	0.72	[0.69, 0.76]	–0.67	[–0.70, 0.64]
Strepsirrhini	0.44	[0.40, 0.48]	0.81	[0.77, 0.84]	–0.66	[–0.69, 0.62]
Intercept						
Catarrhini	–0.03	[–2.31, 2.24]	0.18	[–1.25, 1.59]	–0.09	[–2.00, 1.81]
Platyrrhini	0.30	[–4.29, 4.95]	0.44	[–2.46, 3.30]	–0.69	[–4.49, 3.21]
Strepsirrhini	–0.37	[–5.54, 4.68]	–0.98	[–4.10, 2.22]	1.04	[–3.22, 5.24]

Estimates for the intercepts represent the estimated marginal means calculated by the 'emmeans' function (*emmeans* package). 95% HDI represents the 95% highest density interval. Coefficients of covariates with strong support (i.e., 95% HDI that does not contain zero) are highlighted. All variables were standardized.

Table S15. Summary statistics of Bayesian regressions of the muscle effects modeled as a function of *gape angle* and (*gape angle*)^2 as covariates, and *diet* as a fixed effect.

	Masseter effect		Med. pterygoid effect		Temporalis effect	
Marginal R^2	0.25		0.55		0.39	
Conditional R^2	0.98		0.98		0.98	
Phylogenetic λ	0.88		0.93		0.95	
	Median	**95% HDI**	**Median**	**95% HDI**	**Median**	**95% HDI**
Covariate						
(Gape angle)^2	0.02	[0.01, 0.03]	0.04	[0.03, 0.05]	–0.03	[–0.04, –0.02]
Gape angle						
Folivore	0.32	[0.30, 0.34]	0.73	[0.71, 0.75]	–0.56	[–0.58, –0.54]
Frugivore	0.39	[0.35, 0.44]	0.66	[0.62, 0.70]	–0.58	[–0.62, –0.54]
Frugivore/Folivore	0.44	[0.37, 0.50]	0.69	[0.64, 0.74]	–0.60	[–0.66, –0.54]
Omnivore	0.46	[0.41, 0.51]	0.76	[0.72, 0.81]	–0.64	[–0.68, –0.60]
Intercept						
Folivore	0.19	[–1.18, 1.56]	–0.35	[–1.21, 0.49]	0.20	[–0.85, 1.29]
Frugivore	–0.23	[–2.09, 1.64]	–0.24	[–1.37, 0.87]	0.33	[–1.04, 1.75]
Frugivore/Folivore	–0.81	[–2.73, 1.13]	–0.07	[–1.23, 1.08]	0.57	[–0.84, 2.01]
Omnivore	–0.19	[–2.19, 1.82]	–0.62	[–1.85, 0.58]	0.57	[–0.91, 2.11]

Estimates for the intercepts represent the estimated marginal means calculated by the 'emmeans' function (*emmeans* package). 95% HDI represents the 95% highest density interval. Coefficients of covariates with strong support (i.e., 95% HDI that does not contain zero) are highlighted. All variables were standardized.

Dataset 1.

Available for download at
https://journals.biologists.com/jeb/article-lookup/doi/10.1242/jeb.251335#supplementary-data